

The effect of post-Newtonian spin precessions on the evolution of exomoons' obliquity

Lorenzo Iorio¹

Ministero dell'Istruzione, dell'Università e della Ricerca (M.I.U.R.)
Viale Unità di Italia 68, I-70125, Bari (BA), Italy

lorenzo.iorio@libero.it

Received _____; accepted _____

Abstract

Putative natural massive satellites (exomoons) has gained increasing attention, where they orbit Jupiter-like planets within the habitable zone of their host main sequence star. An exomoon is expected to move within the equatorial plane of its host planet, with its spin S_s aligned with its orbital angular momentum L which, in turn, is parallel to the planetary spin S_p . If, in particular, the common tilt of such angular momenta to the satellite-planet ecliptic plane, assumed fixed, has certain values, the latitudinal irradiation experienced on the exomoon from the star may allow it to sustain life as we know it, at least for certain orbital configurations. An Earth-analog (similar in mass, radius, oblateness and obliquity) is considered, which orbits within 5 – 10 planetary radii R_p from its Jupiter-like host planet. The de Sitter and Lense–Thirring spin precessions due to the general relativistic post-Newtonian (pN) field of the host planet have an impact on an exomoon’s habitability for a variety of different initial spin-orbit configurations. Here, I show it by identifying long-term variations in the satellite’s obliquity ε_s , where variations can be $\lesssim 10^\circ - 100^\circ$, depending on the initial spin-orbit configuration, with a timescale of $\simeq 0.1 - 1$ million years. Also the satellite’s quadrupole mass moment J_2^s induces obliquity variations which are faster than the pN ones, but do not cancel them.

Subject headings: Planets and satellites: general – Astrobiology – Gravitation – Celestial mechanics – Methods: analytical – Methods: numerical

1. Introduction

In investigating the possibility that alien worlds, extrasolar planets (Seager 2011; Lissauer 2012; Deeg & Belmonte 2018; Perryman 2018) and related environments, may host and sustain known (and unknown) forms of life and, possibly, civilizations (Kaltenegger 2017; Schulze-Makuch & Bains 2018; Schwieterman et al. 2018; Irwin & Schulze-Makuch 2020), it is of crucial importance to assess the physical conditions posing tight constraints. In this framework, I will look at a novel scenario, where Einstein’s General Theory of Relativity (GTR; Debono & Smoot 2016; Misner, Thorne & Wheeler 2017), along with other classical effects, may have a direct, macroscopic impact on life and its long-term sustainability.

Natural satellites of Jupiter-like gas giants, or exomoons (Barnes & O’Brien 2002; Domingos, Winter & Yokoyama 2006; Heller et al. 2014; Schneider, Lainey & Cabrera 2015), could be habitable if the host planet orbits within the habitable zone of its main sequence star (Williams, Kasting & Wade 1997; Kaltenegger 2010; Heller, R. 2012; Forgan & Kipping 2013; Heller & Barnes 2013; Hinkel & Kane 2013; Heller et al. 2014; Dobos, Heller & Turner 2017; Zollinger, Armstrong & Heller 2017; Hill et al. 2018; Forgan, D. 2019; Martínez-Rodríguez et al. 2019; Lingam & Loeb 2020; Tjoa, Mueller & van der Tak 2020). In the following, quantities pertaining the exomoon, its host planet and the star are labeled with s , p , and S , respectively. Exomoons’ mass M_s should be $0.25 M_{\oplus} \lesssim M_s \lesssim 2 M_{\oplus}$ to sustain life over a billion-year timescale (Heller & Barnes 2013). According to Sasaki, Stewart & Ida (2010), their actual formation around extrasolar giant planets is possible. In general, different mechanisms of formation of extrasolar planets’s satellites have been proposed so far (Barr 2016), including planet-planet collision, able to create satellites around rocky or icy planets (Barr & Bruck Syal 2017; Malamud et al. 2020), and co-accretion and capture which should lead to gas giants’ exomoons (Heller et al. 2014; Barr 2016). Still unconfirmed exomoons candidates exist (Fox & Wiegert 2021; Teachey & Kipping 2018). The project Hunt for Exomoons with Kepler (HEK) was the most important effort aimed to detect exomoons to date (Kipping et al. 2012, 2013b,a; Teachey, Kipping & Schmitt 2018). Searches for exomoons started in 2009 (Kipping 2009a,b; Kipping, Fossey & Campanella 2009), after theoretical investigations about such a possibility (Sartoretti & Schneider 1999; Cabrera & Schneider 2007). Techniques to be used in exomoons’ detection are transit timing variations (TTVs), transit duration variations (TDVs), and apparent planetary transit radius variations (TRVs) (Rodenbeck, Heller & Gizon 2020); according to Rodenbeck, Heller & Gizon (2020), TRVs could be a more promising means to identify exomoons in large exoplanet surveys.

Such exomoons could be tidally locked to their parent planet but not to the host star, and moving in the planetary equatorial plane due to tidal evolution (Porter & Grundy 2011; Heller & Barnes 2013). Moreover, the satellite’s spin S_s should be parallel to the orbital angular momentum L of the planetocentric motion (Heller & Barnes 2013). Thus, the exomoon should have the same obliquity with respect to the circumstellar orbit as the planetary spin S_p (Heller & Barnes 2013), so that it could experience seasons if the equator of the host planet is tilted against the ecliptic plane (Heller & Barnes 2013). This scenario is plausible because previous studies have shown that exomoons can maintain significant obliquities on large timescales (Heller, Leconte & Barnes

2011; Heller & Barnes 2013).

One of the key parameters for the long-term habitability of an astronomical major body is the axial tilt ε , or obliquity, of its spin to its orbital plane, and its long-term stability over the æons. In the case of a star-planet scenario, the planetary axial tilt ε to the ecliptic plane is crucial for the latitude-dependent insolation received from the host star (Laskar, Joutel & Robutel 1993; Williams & Kasting 1997; Laskar et al. 2004; Armstrong et al. 2014; Linsenmeier, Pascale & Lucarini 2015; Quarles et al. 2019; Kilic, Raible & Stocker 2017; Shan & Li 2018; Quarles, Li & Lissauer 2019). Indeed, variations in obliquity, meant as difference between its extreme values, drive changes in planetary climate. If the obliquity variations are rapid and/or large, the resulting climate shifts can be commensurately severe (Armstrong, Leovy & Quinn 2004). As far as the Earth is concerned, its obliquity changes slowly with time from $\approx 22^\circ.1$ to $24^\circ.5$, undergoing an oscillation cycle with amplitude $\lesssim 2^\circ.4$ in about 41,000 yr (Quarles, Li & Lissauer 2019). The value of the Earth’s obliquity impacts the seasonal cycles and its long-term variation affects the terrestrial climate (Milankovitch 1941), as deduced from geologic records (Kerr 1987; Mitrovica & Forte 1995; Pais et al. 1999). For an exomoon, tidal heating, reflected light by the planet, and the planet’s own infrared irradiation affects the total energy budget in addition to the direct stellar radiation (Heller & Barnes 2013). Thus, it is arguable that the long-term changes of the obliquity ϑ_s relative to the circumplanetary orbital plane will also affect the climate of the exomoon in addition to those of the obliquity ε_s with respect to the ecliptic plane.

The purpose of this paper is to show that GTR may concur to directly affect the habitability of an exomoon through the gravitoelectric de Sitter (de Sitter 1916; Schouten 1918; Fokker 1920) and gravitomagnetic Lense-Thirring¹ (Pugh 1959; Schiff 1960) rates of change of its spin S_s relative to the ecliptic along with other possible classical precessions due to, e.g., tidal friction, quadrupole mass moments J_2^p , J_2^s of the planet and the satellite, 3rd-body effects due to the distant star and other major bodies in the system. They are induced by the post-Newtonian (pN) static and stationary components of the gravitational field of its parent planet (Ohanian & Ruffini 2013; Poisson & Will 2014). To the benefit of a reader not acquainted with GTR, the pN expansion is one of the most successful and famous approximation schemes that have been developed in the past years for solving the fully nonlinear Einstein’s equations to describe motions of arbitrary shaped, massive bodies (Asada & Futamase 1997; Blanchet 2003; Will 2018). Furthermore, the terms “gravitoelectric” and “gravitomagnetic” have nothing to do with electric charges and currents, referring, instead, to the formal resemblance of the linearized Einstein field equations of GTR, valid in the slow-motion and weak-field approximation, with the linear Maxwellian equations of electromagnetism (Thorne, MacDonald & Price 1986; Mashhoon 2001; Rindler 2001). Both such effects were successfully measured some years ago in the dedicated spaceborne experiment Gravity Probe B (GP-B) with four artificial gyroscopes orbiting in the field of the

¹Such a denomination for the pN spin precession induced by the primary’s angular momentum has become of common use, despite it was discovered by Pugh and Schiff in the sixties of the twentieth century.

Earth (Everitt et al. 2011, 2015). The de Sitter precession was detected also by monitoring the heliocentric motion of the Earth-Moon system (Williams, Newhall & Dickey 1996; Williams & Folkner 2009; Hofmann & Müller 2018), thought of as a giant natural gyroscope, with the Lunar Laser Ranging (LLR) technique (Dickey et al. 1994), and in some binary pulsar systems as well (Breton et al. 2008; Kramer 2012).

I will adopt the scenario by Heller & Barnes (2013) consisting of a main sequence star S orbited at 1 astronomical unit (au) by a gravitationally bound restricted two-body system \mathcal{S} made of a Jupiter-like planet p and an Earth-mass exomoon s which, under not too restrictive assumptions, may harbour life. In fact, exomoons may exist also in the habitable zone of M dwarfs (Martínez-Rodríguez et al. 2019; Trifonov et al. 2020), but, in this case, the analysis would be more involved because of the direct dynamical and tidal effects of the star itself. It will be shown that, for the range of plausible distances allowed to the exomoon in order to be habitable (Heller & Barnes 2013) and a variety of different initial spin-orbit configurations, ε_s may undergo pN variations $\Delta\varepsilon_s$ with respect to its initial value ε_0^s of tens and even hundreds of degrees depending on the spin-orbit configuration over $\simeq 0.1 - 1$ Myr. I will neglect the presence of other planets in the system, so that the ecliptic plane, assumed as reference coordinate $\{x, y\}$ plane, stays essentially fixed. The orbit of the exomoon around its host planet will be circular, with a size of 5 to 10 planetary radii R_p (Heller & Barnes 2013). As far as the exomoon’s primary is concerned, I will, first, assume the physical parameters of Jupiter. Then, I will look also at other more massive, larger and more rapidly spinning prototypical gaseous giant planet having the properties of one of those recently characterized in Bryan et al. (2020). It should be stressed that, by placing the planet-satellite system at 1 au from the star, the GTR spin precessions considered here are not due to the pN components of the star’s gravitational field; moreover, it can be reasonably assumed that the ecliptic plane is not perturbed too much by the post-Keplerian (pK), Newtonian or pN, components of the stellar field which, in principle, are able to induce long-term orbital variations. Instead, they are induced by the planet’s pN field itself; thus, the sources of the de Sitter and Lense-Thirring precessions of the exomoon’s spin are the mass M_p and the spin angular momentum S_p of the Jupiter-type gas giant, respectively (Ohanian & Ruffini 2013; Poisson & Will 2014). As such, they are present independently of any peculiar characteristic of the exomoon itself like, e.g., its quadrupole mass moment J_2^s , Love number k_2^s , tidal lag time Δt_s (Mignard 1979; Correia et al. 2011; Efroimsky & Makarov 2013), etc., which may induce their own long-term changes in the obliquity of its spin. In a further step, I will include also J_2^s yielding a further direct exomoon’s spin precession characterized by a much higher frequency which does not cancel the pN ones superimposing to them.

The paper is organized as follows. In Section 2, analytical expressions for the pN rates of change of the satellite’s spin axis with respect to a fixed reference plane are derived, and some qualitative features of their solution for ε_s are discussed. They are numerically integrated for the case of a Jupiter-like host planet in Section 3, and for a different gaseous giant body in Section 4 by suitably varying the system’s parameter space in both cases. In Section 5, I deal with the classical spin precession due to the exomoon’s own quadrupole mass moment J_2^s , while Section 6

is devoted to the impact of the distant star and to the obliquity to the planetocentric orbital plane. Section 7 summarizes my findings and offer my conclusions.

2. The de Sitter and Lense-Thirring precessions of the spin's obliquity to the ecliptic plane

2.1. The analytical equations of the pN precessions

Let me assume a coordinate system whose reference $\{x, y\}$ plane coincides with the ecliptic plane of the planet-satellite binary. As parameterization of the satellite's spin axis $\hat{\mathbf{S}}_s$, I adopt

$$\hat{S}_x^s = \sin \varepsilon_s \cos \alpha_s, \quad (1)$$

$$\hat{S}_y^s = \sin \varepsilon_s \sin \alpha_s, \quad (2)$$

$$\hat{S}_z^s = \cos \varepsilon_s, \quad (3)$$

so that α_s is the spin's azimuthal angle and ε_s is its obliquity to the ecliptic: $\varepsilon_s = 0^\circ$ means that the spin is perpendicular to it. From Equations (1)-(3), it can be straightforwardly obtained

$$\frac{d\varepsilon_s}{dt} = -\csc \varepsilon_s \frac{d\hat{S}_z^s}{dt}, \quad (4)$$

$$\frac{d\alpha_s}{dt} = \csc \varepsilon_s \left(\cos \alpha_s \frac{d\hat{S}_y^s}{dt} - \sin \alpha_s \frac{d\hat{S}_x^s}{dt} \right). \quad (5)$$

To the pN order, the general relativistic rates of change of ε_s , α_s , averaged over one orbital revolution of the satellite about its parent planet, can be inferred from the sum of the pN de Sitter and Lense-Thirring averaged precessions of $\hat{\mathbf{S}}_s$

$$\frac{d\hat{\mathbf{S}}_s}{dt} = \left(\boldsymbol{\Omega}_{\text{ds}}^s + \boldsymbol{\Omega}_{\text{LT}}^s \right) \times \hat{\mathbf{S}}_s, \quad (6)$$

where (Barker & O'Connell 1975; Poisson & Will 2014)

$$\boldsymbol{\Omega}_{\text{ds}}^s = \frac{3 n_b \mu_p}{2 c^2 a (1 - e^2)} \hat{\mathbf{L}}, \quad (7)$$

$$\boldsymbol{\Omega}_{\text{LT}}^s = \frac{G S_p}{2 c^2 a^3 (1 - e^2)^{3/2}} \left[\hat{\mathbf{S}}_p - 3 (\hat{\mathbf{S}}_p \cdot \hat{\mathbf{L}}) \hat{\mathbf{L}} \right]. \quad (8)$$

In Equations (7)-(8), c is the speed of light in vacuum, G is the Newtonian gravitational constant, $\mu_p \doteq G M_p$ is the planet's gravitational parameter, a , e are the semimajor axis and the eccentricity, respectively, of the satellite's planetocentric orbit, $n_b = \sqrt{\mu_p/a^3}$ is the Keplerian mean motion, $\hat{\mathbf{L}} = \{\sin I \sin \Omega, -\sin I \cos \Omega, \cos I\}$ is the unit vector of the orbital angular momentum, I is the inclination of the satellite's orbital plane to the ecliptic, and Ω is its longitude of the ascending node. By parameterizing the planet's spin axis $\hat{\mathbf{S}}_p$ as

$$\hat{S}_x^p = \sin \varepsilon_p \cos \alpha_p, \quad (9)$$

$$\hat{S}_y^p = \sin \varepsilon_p \sin \alpha_p, \quad (10)$$

$$\hat{S}_z^p = \cos \varepsilon_p, \quad (11)$$

where ε_p , α_p are its obliquity and azimuthal angle, respectively, from Equations (1)-(11), one finally gets

$$\begin{aligned} \frac{d\varepsilon_s}{dt} = & -\frac{3 n_b \mu_p \sin I \cos \zeta_s}{2 c^2 a (1 - e^2)} + \\ & + \frac{G S_p}{4 c^2 a^3 (1 - e^2)^{3/2}} \left[\sin \varepsilon_p \left(\sin \Delta\alpha_{sp} - 3 \sin \chi_{sp} \right) + 3 \cos \zeta_s \left(\cos \varepsilon_p \sin 2I + 2 \cos^2 I \sin \varepsilon_p \sin \zeta_p \right) \right], \end{aligned} \quad (12)$$

$$\begin{aligned} \frac{d\alpha_s}{dt} = & \frac{3 n_b \mu_p (\cos I + \cot \varepsilon_s \sin I \sin \zeta_s)}{2 c^2 a (1 - e^2)} - \\ & - \frac{G S_p}{8 c^2 a^3 (1 - e^2)^{3/2}} \left\{ \cos \varepsilon_p \left(2 + 6 \cos^2 I - 6 \sin^2 I + 6 \cot \varepsilon_s \sin 2I \sin \zeta_s \right) + \right. \\ & \left. + \sin \varepsilon_p \left[\left(\cos \Delta\alpha_{sp} + 3 \cos \chi_{sp} \right) \cot \varepsilon_s - 6 \left(\sin 2I - \cos 2I \cot \varepsilon_s \sin \zeta_s \right) \sin \zeta_p \right] \right\}, \end{aligned} \quad (13)$$

with

$$\zeta_s \doteq \alpha_s - \Omega, \quad (14)$$

$$\zeta_p \doteq \alpha_p - \Omega, \quad (15)$$

$$\chi_{sp} \doteq \zeta_s + \zeta_p, \quad (16)$$

$$\Delta\alpha_{sp} \doteq \alpha_s - \alpha_p. \quad (17)$$

Equations (14)-(16) are relative nodes. In terms of the parameterization of Equations (1)-(3) and Equations (9)-(11), the azimuthal angle Ξ of $\hat{\mathbf{L}}$ is related to Ω by

$$\Omega = 90^\circ + \Xi. \quad (18)$$

If $\hat{\mathbf{S}}_s$, $\hat{\mathbf{L}}$, $\hat{\mathbf{S}}_p$ are aligned with each other, i.e. for $\varepsilon_s = I = \varepsilon_p$ and $\alpha_s = \Xi = \alpha_p$, it is

$$\zeta_s = \zeta_p = -90^\circ, \quad (19)$$

$$\chi_{sp} = -180^\circ, \quad (20)$$

$$\Delta\alpha_{sp} = 0, \quad (21)$$

so that Equations (12)-(13) vanish.

In obtaining the averaged rates of Equations (12)-(13), it was assumed that ε_s , α_s stay essentially constant over one satellite's orbital period, and that I , Ω are fixed, i.e. a Keplerian ellipse was used as unperturbed, reference trajectory in the averaging procedure. Such an assumption is justified by the fact that the exomoon's orbital period amounts just to a few days, while the characteristic timescale of its spin precession is of the order of $\simeq 0.1 - 1\text{Myr}$ (see Sections 3 to 4). In fact, a long-term modulation is introduced in Equations (12)-(13) by I , Ω since, actually, they do vary because of a number of classical and general relativistic pK precessions the most important of which are the classical ones due to the planetary oblateness J_2^p and the pN Lense-Thirring effect caused by the planet's spin S_p . Their characteristic timescales are much longer than the orbital period by several orders of magnitude since they can be calculated perturbatively by averaging out their Gauss equations over one orbital revolution; the quadrupolar and the Lense-Thirring accelerations (Brumberg 1991; Soffel & Han 2019) are, indeed, orders of magnitude smaller than the Newtonian monopole one. By using Equations (1)-(3) and Equations (9)-(11), the classical and relativistic pK averaged rates of change of I , Ω for an arbitrary orientation of the primary's spin axis (Barker & O'Connell 1975; Damour & Schafer 1988; Damour & Taylor 1992; Will 2008; Iorio 2017)

$$\frac{dI}{dt} = -\frac{3 n_b R_p^2 J_2^p (\hat{\mathbf{S}}_p \cdot \hat{\mathbf{N}}) (\hat{\mathbf{S}}_p \cdot \hat{\mathbf{L}})}{2 a^2 (1 - e^2)^2} + \frac{2 G S_p (\hat{\mathbf{S}}_p \cdot \hat{\mathbf{N}})}{c^2 a^3 (1 - e^2)^{3/2}}, \quad (22)$$

$$\frac{d\Omega}{dt} = -\frac{3 n_b R_p^2 J_2^p \csc I (\hat{\mathbf{S}}_p \cdot \hat{\mathbf{M}}) (\hat{\mathbf{S}}_p \cdot \hat{\mathbf{L}})}{2 a^2 (1 - e^2)^2} + \frac{2 G S_p \csc I (\hat{\mathbf{S}}_p \cdot \hat{\mathbf{M}})}{c^2 a^3 (1 - e^2)^{3/2}}, \quad (23)$$

where $\hat{\mathbf{N}} = \{\cos \Omega, \sin \Omega, 0\}$ is the unit vector directed along the line of the nodes, which is the intersection of the satellite's orbital plane with the ecliptic, toward the longitude of the ascending node, and $\hat{\mathbf{M}} = \{-\cos I \sin \Omega, \cos I \cos \Omega, \sin I\}$ is the unit vector directed in the orbital plane

such that $\hat{N} \times \hat{M} = \hat{L}$, can be cast into the form

$$\begin{aligned} \frac{dI}{dt} = & \frac{3 n_b R_p^2 J_2^p \cos \zeta_p \sin \varepsilon_p \left(-\cos I \cos \varepsilon_p + \sin I \sin \varepsilon_p \sin \zeta_p \right)}{2 a^2 (1 - e^2)^2} + \\ & + \frac{2 G S_p \sin \varepsilon_p \cos \zeta_p}{c^2 a^3 (1 - e^2)^{3/2}}, \end{aligned} \quad (24)$$

$$\begin{aligned} \frac{d\Omega}{dt} = & -\frac{3 n_b R_p^2 J_2^p \sin I \left(\cos \varepsilon_p + \cot I \sin \varepsilon_p \sin \zeta_p \right) \left(\cot I \cos \varepsilon_p - \sin \varepsilon_p \sin \zeta_p \right)}{2 a^2 (1 - e^2)^2} + \\ & + \frac{2 G S_p \left(\cos \varepsilon_p + \cot I \sin \varepsilon_p \sin \zeta_p \right)}{c^2 a^3 (1 - e^2)^{3/2}}. \end{aligned} \quad (25)$$

Equations (22)-(23) can be expressed in compact, vectorial form as (Barker & O’Connell 1975)

$$\frac{d\hat{L}}{dt} = \left(\Omega_{\text{ds}}^L + \Omega_{\text{LT}}^L + \Omega_{\text{obl}}^L \right) \times \hat{L}, \quad (26)$$

where

$$\Omega_{\text{ds}}^L = 2 \Omega_{\text{ds}}^s, \quad (27)$$

$$\Omega_{\text{LT}}^L = 4 \Omega_{\text{LT}}^s, \quad (28)$$

$$\Omega_{\text{obl}}^L = -\frac{3 n_b J_2^p R_p^2}{4 a^2 (1 - e^2)^2} \left\{ 2 (\hat{S}_p \cdot \hat{L}) \hat{S}_p + \left[1 - 5 (\hat{S}_p \cdot \hat{L})^2 \right] \hat{L} \right\}. \quad (29)$$

Note that Equations (27)-(29) strictly hold in the test particle limit of the full two-body expressions by Barker & O’Connell (1975). Equations (24)-(25) vanish for Equations (19)-(20). Thus, also the orbital angular momentum stay fixed in space if \hat{S}_s , \hat{L} , \hat{S}_p are aligned, as it can straightforwardly be inferred from Equations (7)-(8), Equation (29) and Equation (26).

Equations (12)-(13) and Equations (24)-(25) represent a system of nonlinear first order differential equations for the four unknowns ε_s , α_s , I , Ω to be simultaneously integrated; ε_p , α_p are assumed to be constant.

2.2. Some qualitative features of the pN obliquity precessions

In order to grasp some essential features of the numerically integrated time series displayed in Sections 3 to 4, I will make some considerations about Equations (12)-(13) and

Equations (24)-(25).

Let me define

$$\nu_{\text{dS}} \doteq \frac{3 n_b \mu_p}{2 c^2 a (1 - e^2)}, \quad (30)$$

$$\nu_{\text{LT}} \doteq \frac{G S_p}{c^2 a^3 (1 - e^2)^{3/2}}, \quad (31)$$

$$\nu_{\text{obl}} \doteq \frac{3 n_b J_2^p R_p^2}{2 a^2 (1 - e^2)^2}, \quad (32)$$

so that

$$\Lambda_{\text{dS}}^{\text{LT}} \doteq \frac{\nu_{\text{LT}}}{\nu_{\text{dS}}} = \frac{2 S_p}{3 \sqrt{M_p^3 G a (1 - e^2)}}, \quad (33)$$

$$\Delta_{\text{obl}}^{\text{LT}} \doteq \frac{2 \nu_{\text{LT}}}{\nu_{\text{obl}}} = \frac{4 G S_p \sqrt{1 - e^2}}{3 c^2 a n_b R_p^2 J_2^p}, \quad (34)$$

$$\Gamma_{\text{dS}}^{\text{obl}} \doteq \frac{\nu_{\text{obl}}}{\nu_{\text{dS}}} = \frac{c^2 J_2^p R_p^2}{\mu_p a (1 - e^2)}. \quad (35)$$

For a circular orbit at $5 R_p \leq a \leq 10 R_p$ from a Jupiter-like host planet, it is

$$\Lambda_{\text{dS}}^{\text{LT}} \simeq 0.03, \quad (36)$$

$$\Delta_{\text{obl}}^{\text{LT}} \simeq 5 \times 10^{-7}, \quad (37)$$

$$\Gamma_{\text{dS}}^{\text{obl}} \simeq 10^5. \quad (38)$$

It implies that, in the considered scenario and over timescales shorter than the gravitomagnetic characteristic ones, the Lense-Thirring spin and orbital precessions can generally be neglected with respect to the de Sitter and quadrupolar ones, respectively, apart from some particular spin and orbital configurations. Also in such an approximated case, it is not possible to obtain analytical solutions from the simultaneous integration of Equations (12)-(13) and Equations (24)-(25) for an arbitrary spin-orbit configuration. Nonetheless, some qualitative features, which will allow to understand certain aspects of the numerically integrated time series in Section 4 with respect to

those in Section 3, can still be inferred. Equations (12)-(13) can be combined obtaining

$$\frac{d\varepsilon_s}{d\alpha_s} \simeq -\frac{\tan I \cos \zeta_s}{1 + \tan I \cot \varepsilon_s \sin \zeta_s}, \quad (39)$$

where

$$\frac{d\alpha_s}{dt} \simeq v_{\text{dS}} \cos I (1 + \tan I \cot \varepsilon_s \sin \zeta_s). \quad (40)$$

Equation (39) implies that, whether I and Ω vary or not, the amplitude of $\varepsilon(\alpha_s)$ is independent of either the exomoon's distance from the planet and the physical parameters of the latter up to the order of $O(\Lambda_{\text{dS}}^{\text{LT}})$, depending only on the initial spin-orbit configuration. Furthermore, Equation (40) tells that, however complicated the dependence of α_s on t may be, the characteristic time scale of the resulting time series of $\varepsilon_s(t)$, which is generally not a simple harmonic function, is determined by Equation (30). Such features can be explicitly inferred in some particular cases like, e.g., in a purely de Sitter scenario. According to Equations (24)-(25), it is $I = I_0$, $\Omega = \Omega_0$ for $J_2^{\text{p}} = 0$, $S_{\text{p}} = 0$. Then, by analytically solving Equation (6) with Equation (7) only, it is possible to obtain

$$\begin{aligned} \hat{S}_z^{\text{s}}(t) = \cos \varepsilon_s(t) = & \cos^2 I_0 \cos \varepsilon_s^0 + \cos \varepsilon_s^0 \cos(v_{\text{dS}} t) \sin^2 I_0 + \sin \varepsilon_s^0 \left[\cos \zeta_s^0 \sin I_0 \sin(v_{\text{dS}} t) - \right. \\ & \left. - \sin 2I_0 \sin^2\left(\frac{v_{\text{dS}}}{2} t\right) \sin \zeta_s^0 \right], \end{aligned} \quad (41)$$

where $\zeta_s^0 \doteq \alpha_s^0 - \Omega_0$.

3. The case of a Jupiter-like parent planet

I numerically integrated Equations (12)-(13) along with Equations (24)-(25) over 1 Myr for a fictitious exomoon circling a planet with the same physical parameters of Jupiter along a circular orbit at a few radii from it, as per Heller & Barnes (2013). About the initial conditions, I, first, looked at different mutual orientations of \hat{S}_s , \hat{L} , \hat{S}_p for a fixed satellite's planetocentric distance $a = 5 R_{\text{p}}$; restricting only to, say, a Jupiter-Io scenario would not be justified by the different possible formation mechanisms of exomoons, by the variety of spin-orbit configurations in several star-exoplanet systems discovered so far (Campante et al. 2016), and by the fact that, until now, no exomoons have yet been unquestionably detected. Then, in Figure 5, I varied a from $5 R_{\text{p}}$ to $10 R_{\text{p}}$ for a given spin-orbit configuration.

The case of a close, although not perfect, mutual alignment of \hat{L} , \hat{S}_p , \hat{S}_s is shown in Figure 1, based on the initial conditions of Table 1. I allowed for offsets of a few degrees among the spherical angles of the three angular momenta with respect to, say, $\{\theta\} = 23^{\circ}.44$, $\{\phi\} = 150^{\circ}$, where $\{\theta\} \doteq \varepsilon_s^0$, I_0 , ε_{p} and $\{\phi\} = \alpha_s^0$, Ξ_0 , α_{p} . The resulting ranges $\varepsilon_s^{\text{max}} - \varepsilon_s^{\text{min}}$ of the time series of Figure 1 are still potentially significant for life since their sizes are of the order of $\simeq 3^{\circ} - 17^{\circ}$ over characteristic timescales as short as 0.7 Myr, as resumed in Table 1.

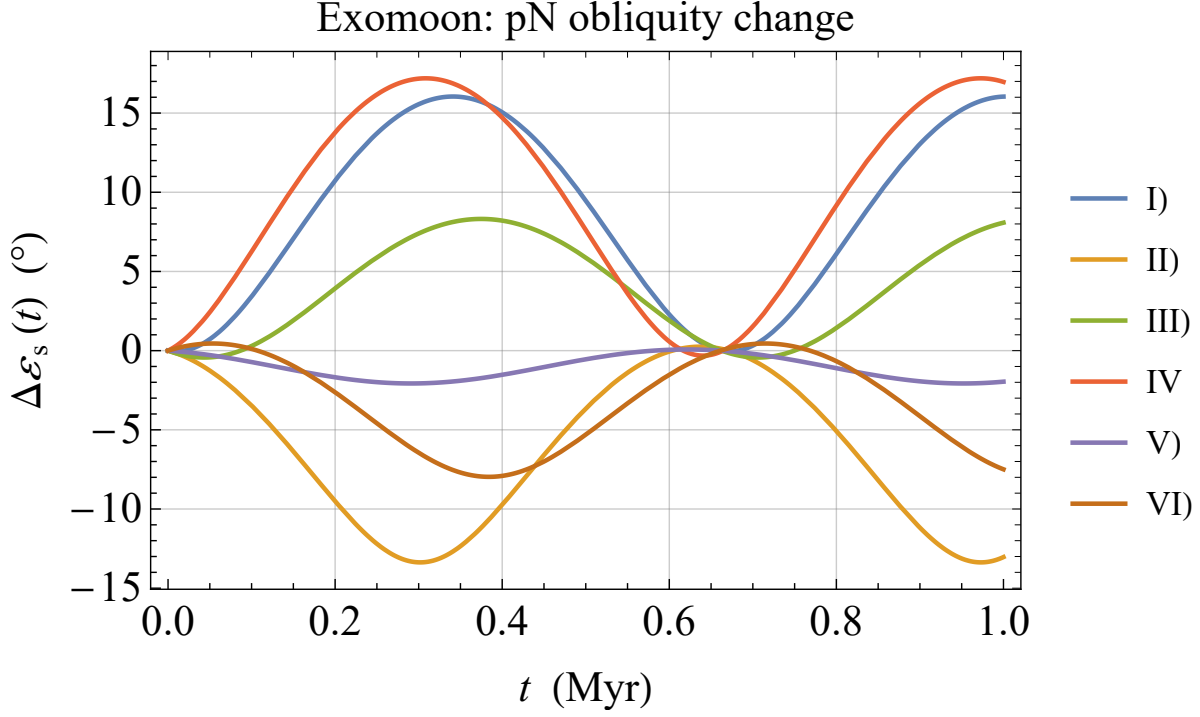


Fig. 1.— Numerically produced time series $\Delta\varepsilon_s(t) = \varepsilon_s(t) - \varepsilon_s^0$, in $^\circ$, of the general relativistic pN variation of the obliquity ε_s to the ecliptic plane of a putative exomoon orbiting a gaseous giant planet with the same physical properties of Jupiter. They were obtained by simultaneously integrating the orbit-averaged Equations (12)-(13) and Equations (24)-(25) for the rates of change of ε_s , α_s , Ω , I over 1 Myr. The initial conditions, corresponding to a close alignment of $\hat{\mathbf{L}}$, $\hat{\mathbf{S}}_p$, $\hat{\mathbf{S}}_s$, are listed in Table 1, which summarizes the main features of the signatures as well.

Table 2 and Figure 2 deal with the case in which the three angular momenta initially share

Table 1: Initial conditions used in Figure 1. Each row corresponds to the plotted times series with the same roman numeral in the legend of Figure 1. Recall that the azimuthal angle of $\hat{\mathbf{L}}$ is $\Xi = \Omega - 90^\circ$. T is the characteristic timescale, and $\varepsilon_s^{\max} - \varepsilon_s^{\min}$ is the full range of variation of the exomoon’s obliquity to the ecliptic.

	$a (R_p)$	e	$I_0 (^\circ)$	$\Omega_0 (^\circ)$	$\varepsilon_p (^\circ)$	$\alpha_p (^\circ)$	$\varepsilon_s^0 (^\circ)$	$\alpha_s^0 (^\circ)$	T (Myr)	$\varepsilon_s^{\max} - \varepsilon_s^{\min} (^\circ)$
I)	5	0.0	25 $^\circ$:44	233	29 $^\circ$:44	147	21 $^\circ$:44	149	0.7	16
II)	5	0.0	28 $^\circ$:44	243	18 $^\circ$:44	146	25	151	0.7	13
III)	5	0.0	22 $^\circ$:44	248	24 $^\circ$:44	148	20.50	153	0.7	10
IV)	5	0.0	21 $^\circ$:7	242	27 $^\circ$:44	156	19	150	0.7	17
V)	5	0.0	20 $^\circ$:44	240	22 $^\circ$:44	153	23 $^\circ$:44	154	0.7	3
VI)	5	0.0	19 $^\circ$:44	238	20 $^\circ$:44	152	24 $^\circ$:20	147	0.7	9

almost the same azimuthal plane, being tilted differently to the ecliptic. It can be noted that $\varepsilon_s^{\max} - \varepsilon_s^{\min}$ ranges from 10° to 150° .

Table 2: Initial conditions used in Figure 2. Each row corresponds to the plotted times series with the same roman numeral in the legend of Figure 2. Recall that the azimuthal angle of $\hat{\mathbf{L}}$ is $\Xi = \Omega - 90^\circ$. T is the characteristic timescale, and $\varepsilon_s^{\max} - \varepsilon_s^{\min}$ is the full range of variation of the exomoon’s obliquity to the ecliptic.

	$a (R_p)$	e	$I_0 (^\circ)$	$\Omega_0 (^\circ)$	$\varepsilon_p (^\circ)$	$\alpha_p (^\circ)$	$\varepsilon_s^0 (^\circ)$	$\alpha_s^0 (^\circ)$	T (Myr)	$\varepsilon_s^{\max} - \varepsilon_s^{\min} (^\circ)$
I)	5	0.0	15	233	5	147	80	149	0.7	10
II)	5	0.0	30	243	15	146	65	151	0.7	30
III)	5	0.0	65	248	30	148	50	153	0.7	40
IV)	5	0.0	5	242	50	156	30	150	0.7	40
V)	5	0.0	80	240	65	153	15	154	0.7	100
VI)	5	0.0	50	238	80	152	5	147	0.7	150

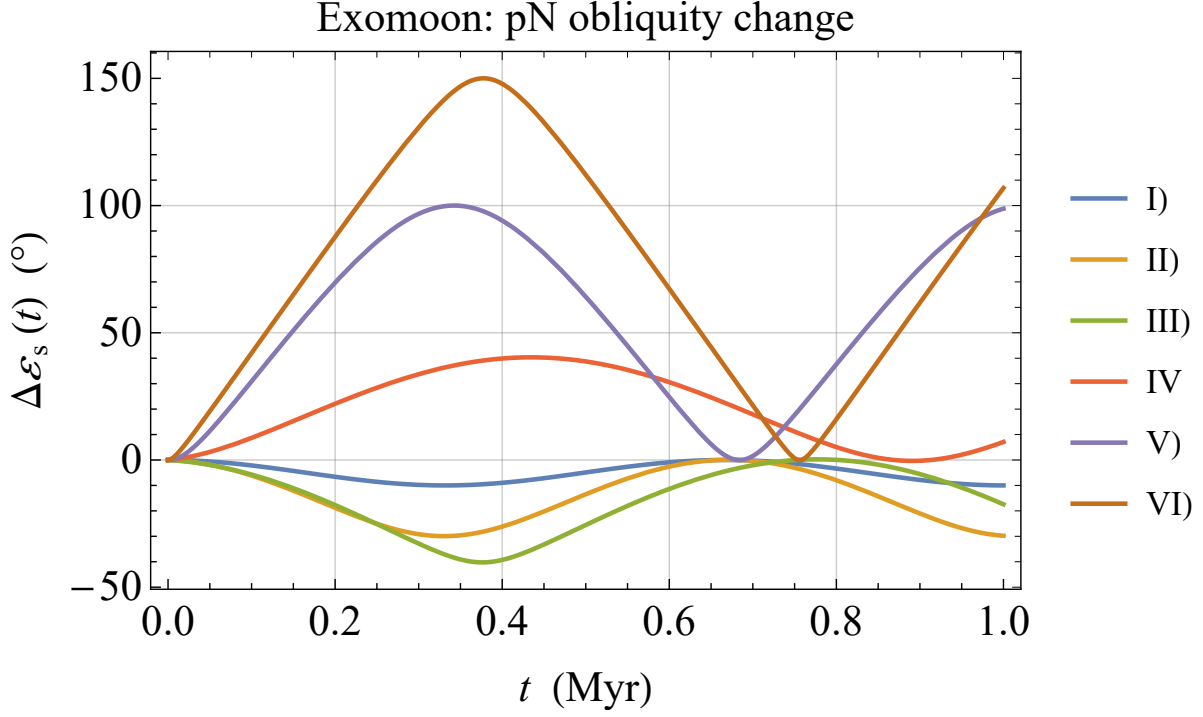


Fig. 2.— Numerically produced time series $\Delta\varepsilon_s(t) = \varepsilon_s(t) - \varepsilon_s^0$, in $^\circ$, of the general relativistic pN variation of the obliquity ε_s to the ecliptic plane of a putative exomoon orbiting a gaseous giant planet with the same physical properties of Jupiter. They were obtained by simultaneously integrating the orbit-averaged Equations (12)-(13) and Equations (24)-(25) for the rates of change of ε_s , α_s , Ω , I over 1 Myr. The initial conditions, corresponding to $\hat{\mathbf{L}}$, $\hat{\mathbf{S}}_p$, $\hat{\mathbf{S}}_s$ lying almost in the same azimuthal plane but tilted differently from each other, are listed in Table 2, which summarizes the main features of the signatures as well.

Table 3 and Figure 3 refer to $\hat{\mathbf{L}}$, $\hat{\mathbf{S}}_p$, $\hat{\mathbf{S}}_s$ sharing almost the same tilt to the ecliptic and displaced in different azimuthal planes. In this case, the range of values for $\Delta\varepsilon_s$ is narrower than in Figures 1 to 2, amounting to $36^\circ \leq \varepsilon_s^{\max} - \varepsilon_s^{\min} \leq 54^\circ$. Nonetheless, it still remains likely significant for the exomoon’s habitability.

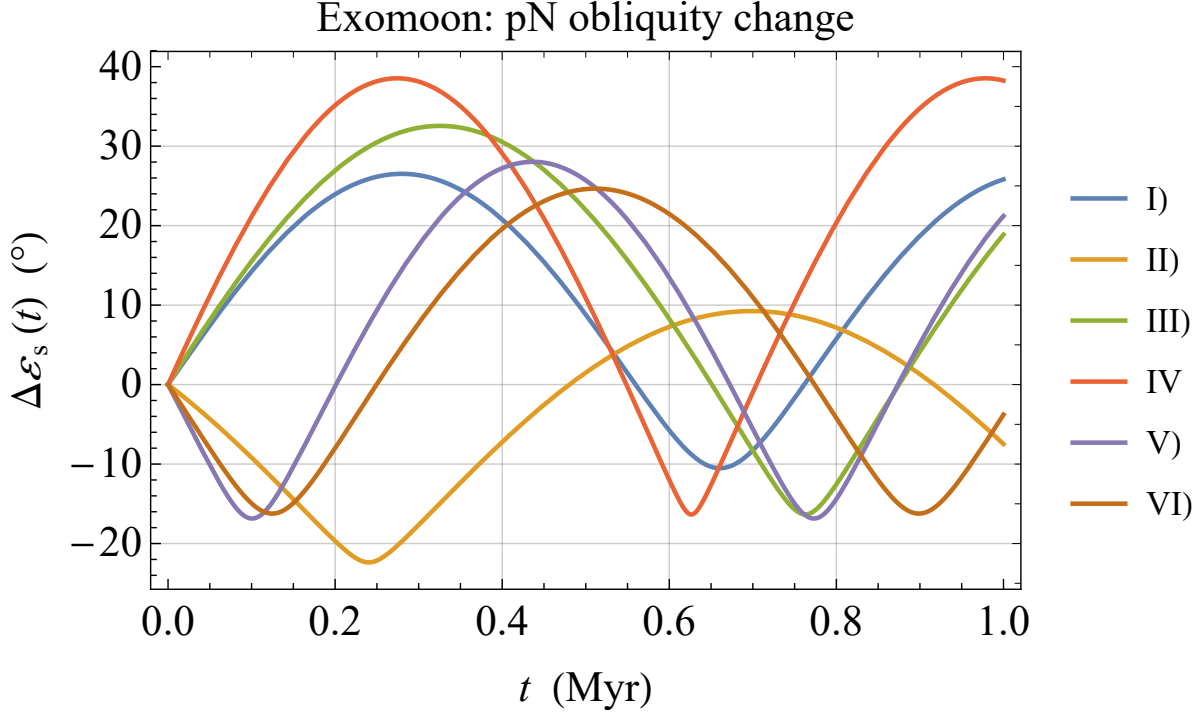


Fig. 3.— Numerically produced time series $\Delta\varepsilon_s(t) = \varepsilon_s(t) - \varepsilon_s^0$, in $^\circ$, of the general relativistic pN variation of the obliquity ε_s to the ecliptic plane of a putative exomoon orbiting a gaseous giant planet with the same physical properties of Jupiter. They were obtained by simultaneously integrating the orbit-averaged Equations (12)-(13) and Equations (24)-(25) for the rates of change of ε_s , α_s , Ω , I over 1 Myr. The initial conditions, corresponding to $\hat{\mathbf{L}}$, $\hat{\mathbf{S}}_p$, $\hat{\mathbf{S}}_s$ tilted almost identically to the ecliptic but located in different azimuthal planes, are listed in Table 3, which summarizes the main features of the signatures as well.

Table 3: Initial conditions used in Figure 3. Each row corresponds to the plotted times series with the same roman numeral in the legend of Figure 3. Recall that the azimuthal angle of $\hat{\mathbf{L}}$ is $\Xi = \Omega - 90^\circ$. T is the characteristic timescale, and $\varepsilon_s^{\max} - \varepsilon_s^{\min}$ is the full range of variation of the exomoon’s obliquity to the ecliptic.

	$a (R_p)$	e	$I_0 (^\circ)$	$\Omega_0 (^\circ)$	$\varepsilon_p (^\circ)$	$\alpha_p (^\circ)$	$\varepsilon_s^0 (^\circ)$	$\alpha_s^0 (^\circ)$	T (Myr)	$\varepsilon_s^{\max} - \varepsilon_s^{\min} (^\circ)$
I)	5	0.0	25 $^\circ$:44	90	29 $^\circ$:44	290	21 $^\circ$:44	250	0.7	37
II)	5	0.0	28 $^\circ$:44	130	18 $^\circ$:44	250	25	290	0.7	36
III)	5	0.0	22 $^\circ$:44	170	24 $^\circ$:44	210	20.50	130	0.7	48
IV)	5	0.0	21 $^\circ$:7	210	27 $^\circ$:44	170	19	90	0.7	54
V)	5	0.0	20 $^\circ$:44	250	22 $^\circ$:44	130	23 $^\circ$:44	210	0.7	44
VI)	5	0.0	19 $^\circ$:44	290	20 $^\circ$:44	90	24 $^\circ$:20	170	0.7	40

The case for an arbitrary mutual orientation of the three angular momenta is displayed by Table 4 and Figure 4. The range of values for the satellite’s obliquity to the ecliptic is $60^\circ - 132^\circ$.

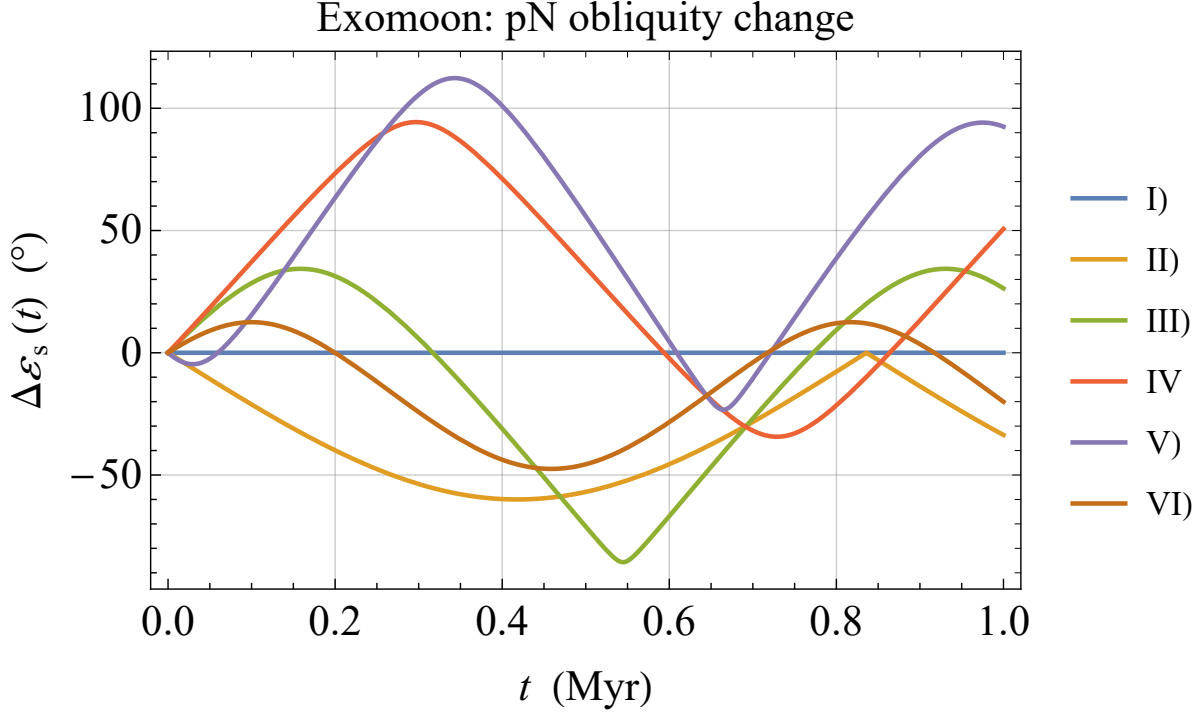


Fig. 4.— Numerically produced time series $\Delta\varepsilon_s(t) = \varepsilon_s(t) - \varepsilon_s^0$, in $^\circ$, of the general relativistic pN variation of the obliquity ε_s to the ecliptic plane of a putative exomoon orbiting a gaseous giant planet with the same physical properties of Jupiter. They were obtained by simultaneously integrating the orbit-averaged Equations (12)-(13) and Equations (24)-(25) for the rates of change of ε_s , α_s , Ω , I over 1 Myr. The initial conditions, corresponding to $\hat{\mathbf{L}}$, $\hat{\mathbf{S}}_p$, $\hat{\mathbf{S}}_s$ arbitrarily oriented, are listed in Table 4, which summarizes the main features of the signatures as well.

Table 4: Initial conditions used in Figure 4. Each row corresponds to the plotted times series with the same roman numeral in the legend of Figure 4. Recall that the azimuthal angle of $\hat{\mathbf{L}}$ is $\Xi = \Omega - 90^\circ$. T is the characteristic timescale, and $\varepsilon_s^{\max} - \varepsilon_s^{\min}$ is the full range of variation of the exomoon’s obliquity to the ecliptic.

	$a (R_p)$	e	$I_0 (^\circ)$	$\Omega_0 (^\circ)$	$\varepsilon_p (^\circ)$	$\alpha_p (^\circ)$	$\varepsilon_s^0 (^\circ)$	$\alpha_s^0 (^\circ)$	T (Myr)	$\varepsilon_s^{\max} - \varepsilon_s^{\min} (^\circ)$
I)	5	0.0	60	0	180	300	150	120	0.7	0.0012
II)	5	0.0	30	60	150	240	180	300	0.7	60
III)	5	0.0	150	120	60	180	90	240	0.7	110
IV)	5	0.0	120	180	90	120	60	0	0.7	120
V)	5	0.0	90	240	120	60	30	180	0.7	132
VI)	5	0.0	180	300	30	0	120	60	0.7	60

In Figure 5, obtained for the initial spin-orbit configuration of Table 5, I varied the satellite’s planetocentric distance from $5 R_p$ to $10 R_p$. As expected from the qualitative analysis of Section 2.2, each time series retains essentially the same maximum range of values $\varepsilon_s^{\max} - \varepsilon_s^{\min} \simeq 180^\circ$, while the characteristic timescales of their temporal patterns, determined by Equation (30), increase with a .

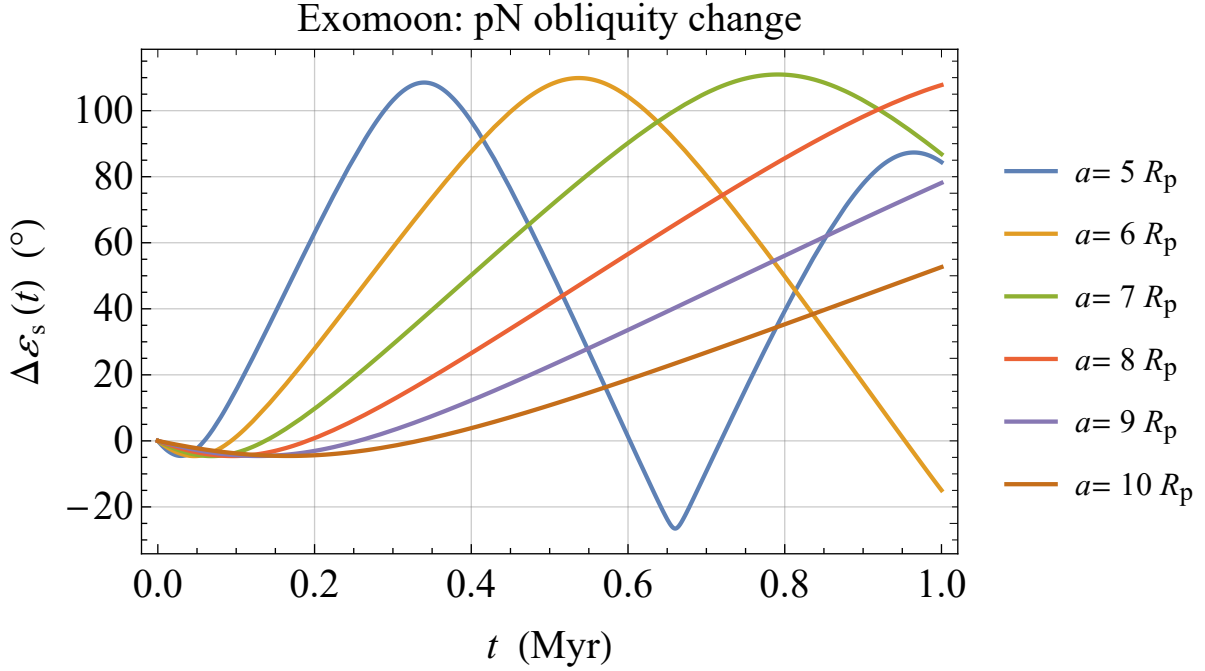


Fig. 5.— Numerically produced time series $\Delta\varepsilon_s(t) = \varepsilon_s(t) - \varepsilon_s^0$, in $^\circ$, of the general relativistic pN variation of the obliquity ε_s to the ecliptic plane of a putative exomoon orbiting a gaseous giant planet with the same physical properties of Jupiter. They were obtained by simultaneously integrating the orbit-averaged Equations (12)-(13) and Equations (24)-(25) for the rates of change of ε_s , α_s , Ω , I over 1 Myr. The initial spin-orbit configuration, common to all the runs, is listed in Table 5.

I checked the validity of Figures 1 to 5, based on the orbit-averaged Equations (12)-(13) and Equations (24)-(25), by numerically integrating the precessional equations of both the satellite’s spin and orbital angular momenta in the vectorial form given by Barker & O’Connell (1975) over the same time spans of the previous runs. In particular, by neglecting all the contributions from the exomoon’s own spin \mathbf{S}_s and quadrupole mass moment J_2^s , I used Equations (7)-(8) for the

Table 5: Initial spin-orbit configuration used in Figure 5.

I_0 ($^\circ$)	Ω_0 ($^\circ$)	ε_p ($^\circ$)	α_p ($^\circ$)	ε_s^0 ($^\circ$)	α_s^0 ($^\circ$)
90	240	120	60	30	180

satellite's spin, and Equations (26)-(29) for the orbital angular momentum. I adopted the same orbital and physical parameters of the previous integrations along with the same initial conditions. Then, I computed the time series for $\varepsilon_s(t)$ from the solution for $\hat{S}_z^s(t)$ as $\varepsilon_s(t) = \arccos \hat{S}_z^s(t)$ by obtaining curves indistinguishable from those in Figures 1 to 5 since they differ, at most, by much less than 1° .

The obliquity ε_s can, in principle, vary also because of torques of classical origin which, however, depend on the peculiar characteristics of the satellite like its own oblateness J_2^s of both tidal and centrifugal origin (Ragozzine & Wolf 2009). Instead, the pN effects previously investigated are due only to the spacetime itself deformed by the mass-energy currents of the parent planet. In Section 5, I will look at the impact of J_2^s as well.

Variations of the latitudinal insolation received by the exomoon from the host star due to changes in ε_s so large as those exhibited by Figures 1 to 5 can certainly have a sensible impact on its habitability, representing a novel element which should be taken into account in future studies on the capability of such worlds to sustain life.

4. The case of faster spinning, larger and more massive gaseous giant planets

Until now, I limited myself to the case of a host planet with the same Jovian physical parameters. It is important to look also at other possible gaseous giants with different fundamental characteristics with respect to Jupiter. Recently, for some of them orbiting at a few tens or hundreds of astronomical units from their parent stars, it was possible to determine some key parameters like the mass M_p , the equatorial radius R_p and the spinning period P_p (Bryan et al. 2020). In order to assess the pN effects on the spin axis of possible exomoons of similar planets, I need estimates of their dimensionless quadrupole mass moment J_2^p and their spin angular momentum S_p .

I will consider a gaseous giant planet with the same characteristics of, say, HD 106906b, whose relevant physical parameters are listed in Table 6. According to known formulas retrievable in, e.g., (Murray & Dermott 2000, Chapter 4), (Helled et al. 2011, Eq. (3)), and (Lissauer, Barnes & Chambers 2012, Appendix A), its J_2^p and S_p turn out to be

$$0.5 \lesssim \frac{J_2^p}{J_2^J} \lesssim 2.5, \quad (42)$$

$$27 \lesssim \frac{S_p}{S_J} \lesssim 45. \quad (43)$$

For Jupiter, it is $J_2^J = 0.0146966$ (Iess et al. 2018), and $S_J = 6.9 \times 10^{38}$ J s (Soffel et al. 2003). The ranges of values in Equations (42)-(43) were obtained for $0.1 \lesssim k_2^p \lesssim 0.6$ (Ragozzine & Wolf 2009), where k_2^p is the planetary Love number (Sterne 1939; Kopal 1959; Ragozzine & Wolf 2009;

Leconte, Lai & Chabrier 2011).

By using the same initial conditions used in Section 3, I numerical integrated Equations (12)-(13) along with Equations (24)-(25) for the planet of Table 6, subsequently confirmed by the integration of the spin and orbit precessional equations in vectorial form by Barker & O’Connell (1975). As expected from the discussion in Section 2.2, the resulting time series are essentially identical to those of Figure 1 to 5, apart from the characteristic timescales which are about one order of magnitude shorter amounting to $\simeq 0.07$ Myr. Indeed, the de Sitter frequency of HD109906b is just 11 times larger than that of Jupiter, being the planetocentric distances the same. Just as an example, in Figure 6, I show the signatures obtained by varying a from $5 R_p$ to $10 R_p$ for the same initial spin-orbit configuration of Table 5. Its resemblance with Figure 5 is remarkable, with the exception of the timescale on the horizontal axis which, in this case, is about 10 times shorter.

Table 6: Mass M_p , equatorial radius R_p , spinning period P_p , dimensionless quadrupole mass moment J_2^p , and spin angular momentum S_p of the gaseous giant planet HD109906b. The values of M_p , R_p , P_p were retrieved from Table 3 of Bryan et al. (2020), while J_2^p , S_p were calculated following, e.g., Bourda & Capitaine (2004); Ragozzine & Wolf (2009); Leconte, Lai & Chabrier (2011) by assuming $k_2^p = 0.52$ (Ragozzine & Wolf 2009) for the planet’s Love number. Here, M_J , R_J , J_2^J , S_J are referred to Jupiter.

$M_p (M_J)$	$R_p (R_J)$	P_p (hr)	$J_2^p (J_2^J)$	$S_p (S_J)$
11	1.56	4	2.2	43.2

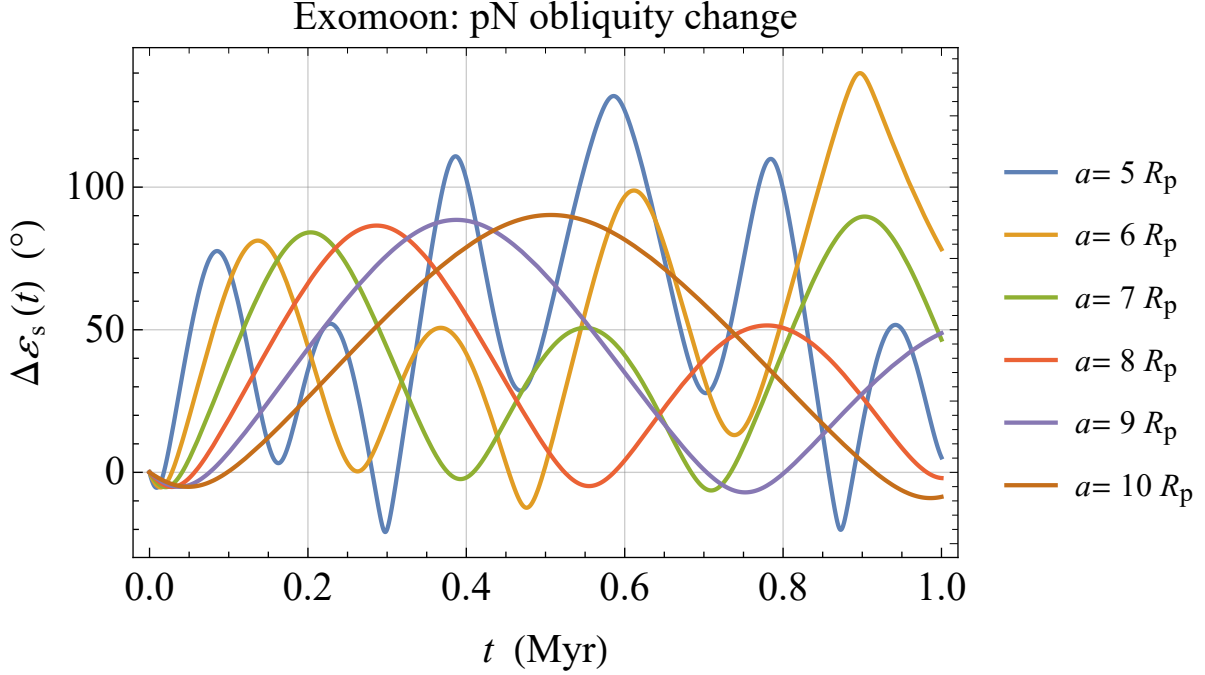


Fig. 6.— Numerically produced time series $\Delta\varepsilon_s(t) = \varepsilon_s(t) - \varepsilon_s^0$, in $^\circ$, of the general relativistic pN variation of the obliquity ε_s to the ecliptic plane of a putative exomoon orbiting a gaseous giant planet with the same physical properties listed in Table 6. They were obtained by simultaneously integrating the orbit-averaged Equations (12)-(13) and Equations (24)-(25) for the rates of change of ε_s , α_s , Ω , I over 1 Myr. The initial spin-orbit configuration, common to all the runs, is listed in Table 5.

5. The impact of the planetary quadrupole mass moment

Here, I will look at the impact of the exomoon’s own oblateness J_2^s on its spin rate.

According to, e.g., Eq. (47) of Barker & O’Connell (1975), the Newtonian satellite’s averaged spin rate due to the gravitational pull of the planet on its equatorial bulge is, in vectorial form,

$$\frac{d\hat{\mathbf{S}}_s}{dt} = \boldsymbol{\Omega}_{\text{obl}}^s \times \hat{\mathbf{S}}_s, \quad (44)$$

with

$$\boldsymbol{\Omega}_{\text{obl}}^s = \frac{\mu_p M_s J_2^s R_s^2}{2 \mathcal{S}_s a^3 (1 - e^2)^{3/2}} [\hat{\mathbf{S}}_s - 3(\hat{\mathbf{S}}_s \cdot \hat{\mathbf{L}}) \hat{\mathbf{L}}]. \quad (45)$$

From Equations (44)-(45) along with Equations (1)-(5) and Equations (9)-(11), one obtains

$$\frac{d\varepsilon_s}{dt} = -\frac{3\mu_p J_2^s M_s R_s^2 \sin I \cos \zeta_s}{2S_s a^3 (1-e^2)^{3/2}} [\cos \zeta_s \sin I (-\cos I \cos \varepsilon_s + \sin I \sin \varepsilon_s \sin \zeta_s)], \quad (46)$$

$$\frac{d\alpha_s}{dt} = -\frac{3\mu_p J_2^s M_s R_s^2 \csc \varepsilon_s}{4S_s a^3 (1-e^2)^{3/2}} [\cos 2\varepsilon_s \sin 2I \sin \zeta_s + \sin 2\varepsilon_s (\cos^2 I - \sin^2 I \sin^2 \zeta_s)], \quad (47)$$

It turns out that, if \hat{S}_s and \hat{L} are aligned, i.e. for $I = \varepsilon_s$, $\zeta_s = -90^\circ$, Equations (46)-(47) vanish. Now, also I and Ω vary because of J_2^s , as shown, e.g., by Eq. (64), Eq. (66), Eq. (71), and Eq. (72) of Barker & O’Connell (1975) or by Eq. (7), Eq. (11), and Eq. (12) of Correia et al. (2011), and of S_s according to Eq. (64), Eq. (66), Eq. (68), and Eq. (69) of Barker & O’Connell (1975) in addition to the changes due to J_2^s , S_p .

In order to include also Equations (46)-(47) in the numerical integrations of Sections 3 to 4, I need quantitative estimates of J_2^s , S_s . The quadrupole mass moment of the exomoon, assumed in hydrostatic equilibrium, can be calculated as (Correia & Rodríguez 2013)

$$J_2^s = \frac{k_2^s}{3} \left(q_c^s - \frac{q_t^s}{2} \right), \quad (48)$$

where

$$q_c^s \doteq \frac{\omega_s^2 R_s^3}{\mu_s} \quad (49)$$

is due to the centrifugal acceleration felt by the satellite, whose gravitational parameter is $\mu_s \doteq G M_s$, spinning at the rate ω_s , while

$$q_t^s \doteq -3 \left(\frac{R_s}{a} \right)^3 \frac{M_p}{M_s} \quad (50)$$

is due to tides raised by the nearby planet. The parameter k_2^s is the exmoon’s Love number which, for a homogeneous solid body, can be calculated as (Murray & Dermott 2000)

$$k_2^s \simeq \frac{3}{2 \left(1 + \frac{19\xi_s}{2\rho_s g_s R_s} \right)}. \quad (51)$$

In Equation (51), ρ_s is the satellite’s mean mass density,

$$g_s \simeq \frac{\mu_s}{R_s^2} \quad (52)$$

is the exmoon’s acceleration of gravity at its surface, and ξ_s is the rigidity of the satellite’s solid core assumed homogeneous and incompressible; for a solid body, it is approximately (Murray & Dermott 2000)

$$\xi_s \simeq 5 \times 10^{10} \text{ N m}^{-2}. \quad (53)$$

The spin angular momentum S_s can be calculated as

$$S_s = j_s M_s R_s^2 \omega_s, \quad (54)$$

where j_s is the normalized moment of inertia (NMoI) which, for a homogenous solid body amounts to $2/5 = 0.4$, being smaller for a differentiated internal structure with an inner compact core (de Pater & Lissauer 2015). In the following, I will adopt the values of the Earth's mass M_\oplus , radius R_\oplus , mean density ρ_\oplus , and NMoI j_\oplus (Petit, Luzum & et al. 2010) for M_s , R_s , ρ_s , j_s , while for the exomoon's angular speed I will assume

$$\omega_s = 1.1 n_b, \quad (55)$$

corresponding to an approximate synchronization with the planetocentric orbital mean motion. Thus, it is

$$0.1 \lesssim \frac{J_2^s}{J_2^\oplus} \lesssim 0.9, \quad (56)$$

$$0.3 \lesssim \frac{S_s}{S_\oplus} \lesssim 0.8 \quad (57)$$

for $5 R_p \leq a \leq 10 R_p$.

By defining

$$\gamma_{\text{obl}}^s \doteq \frac{3 \mu_p J_2^s M_s R_s^2}{2 S_s a^3 (1 - e^2)^{3/2}}, \quad (58)$$

$$\Psi_{\text{obl}}^{\text{dS}} \doteq \frac{\nu_{\text{dS}}}{\gamma_{\text{obl}}^s} = \frac{S_s \sqrt{a (1 - e^2)} \mu_p}{c^2 M_s J_2^s R_s^2}, \quad (59)$$

$$\Pi_{\text{obl}}^{\text{LT}} \doteq \frac{\nu_{\text{LT}}}{\gamma_{\text{obl}}^s} = \frac{2 S_p S_s}{3 c^2 M_p M_s J_2^s R_s^2}, \quad (60)$$

it is possible to repeat the arguments of Section 2.2 applied, now, to the J_2^s -driven rate of change as the fast one and to the pN precessions as slower components. Since for a circular orbit with $5 R_p \leq a \leq 10 R_p$ it is

$$\Psi_{\text{obl}}^{\text{dS}} \simeq 10^{-6}, \quad (61)$$

$$\Pi_{\text{obl}}^{\text{LT}} \simeq 10^{-7}, \quad (62)$$

it turns out that, over timescales much shorter than the characteristic pN ones, the exomoon’s obliquity variations are driven by J_2^s , and their amplitudes depend only on the planet-satellite initial spin-orbit configuration. The dependence on the planet’s physical parameters and on the orbital radius is of the order of $\mathcal{O}(\Psi_{\text{obl}}^{\text{dS}})$, $\mathcal{O}(\Pi_{\text{obl}}^{\text{LT}})$.

Figures 7 to 12, corresponding to the same spin-orbit configurations and the same planet-satellite physical and orbital parameters of Figures 1 to 6, were obtained by simultaneously integrating Equations (12)-(13), Equations (46)-(47), and Equations (24)-(25). It turns out that the exomoon’s oblateness J_2^s introduces high-frequency signatures which superimpose to the pN ones without canceling them. Also in this case, I successfully confirmed such results by numerically integrating the spin rate equations in vectorial form by Barker & O’Connell (1975), whose resulting signatures agree with those in Figures 7 to 12 to within a sub-degree level.

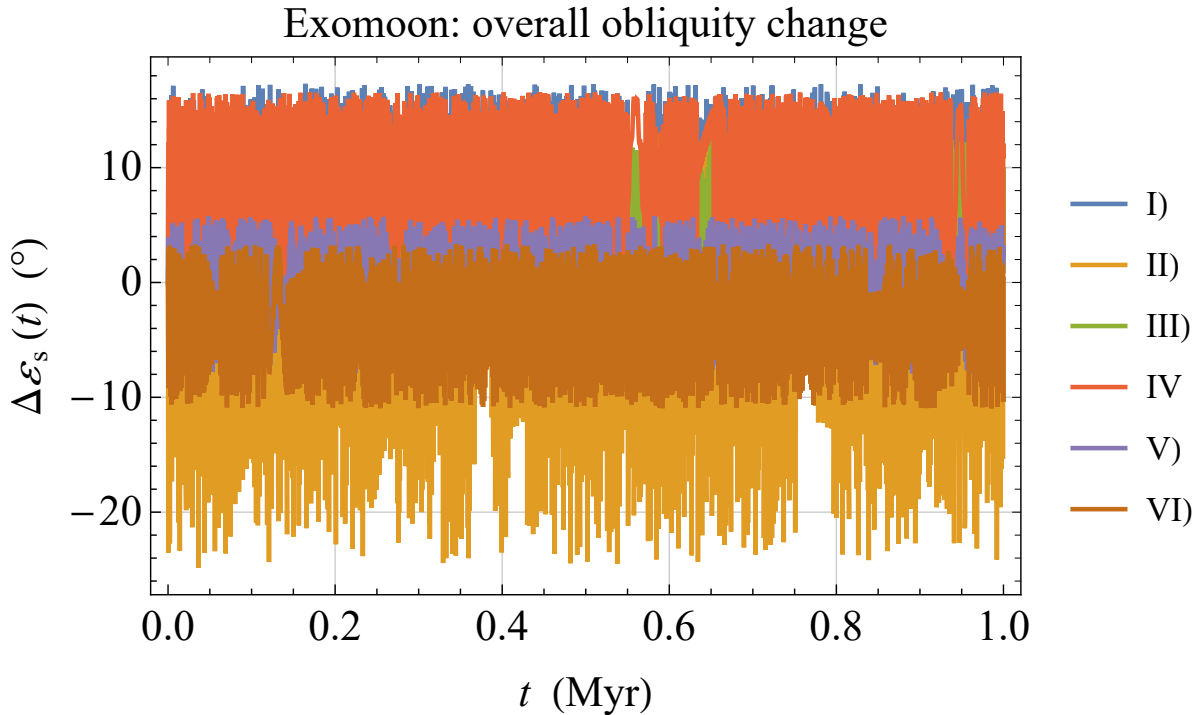


Fig. 7.— Numerically produced time series $\Delta\varepsilon_s(t) = \varepsilon_s(t) - \varepsilon_s^0$, in $^\circ$, of the general relativistic pN variation of the obliquity ε_s to the ecliptic plane of a putative exomoon orbiting a gaseous giant planet with the same physical properties of Jupiter. They were obtained by simultaneously integrating the orbit-averaged Equations (12)-(13), Equations (24)-(25), and Equations (46)-(47) for the rates of change of ε_s , α_s , Ω , I over 1 Myr. The initial conditions, corresponding to a close alignment of $\hat{\mathbf{L}}$, $\hat{\mathbf{S}}_p$, $\hat{\mathbf{S}}_s$, are listed in Table 1. For the exomoon, the mass, radius, normalized moment of inertia and mean density of the Earth were adopted, while $\omega_s = 1.1 n_b$ was assumed for its angular speed.

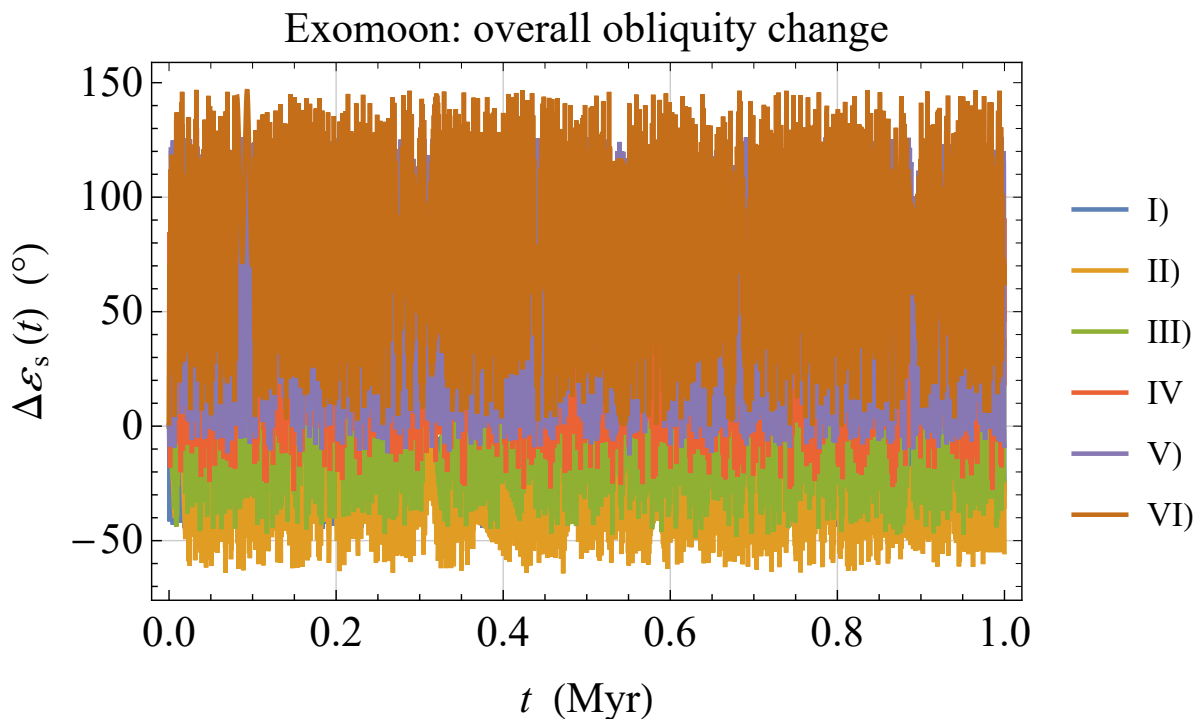


Fig. 8.— Numerically produced time series $\Delta\varepsilon_s(t) = \varepsilon_s(t) - \varepsilon_s^0$, in $^\circ$, of the general relativistic pN variation of the obliquity ε_s to the ecliptic plane of a putative exomoon orbiting a gaseous giant planet with the same physical properties of Jupiter. They were obtained by simultaneously integrating the orbit-averaged Equations (12)-(13), Equations (24)-(25), and Equations (46)-(47) for the rates of change of ε_s , α_s , Ω , I over 1 Myr. The initial conditions, corresponding to $\hat{\mathbf{L}}$, $\hat{\mathbf{S}}_p$, $\hat{\mathbf{S}}_s$ lying almost in the same azimuthal plane but tilted differently from each other, are listed in Table 2. For the exomoon, the mass, radius, normalized moment of inertia and mean density of the Earth were adopted, while $\omega_s = 1.1 n_b$ was assumed for its angular speed.

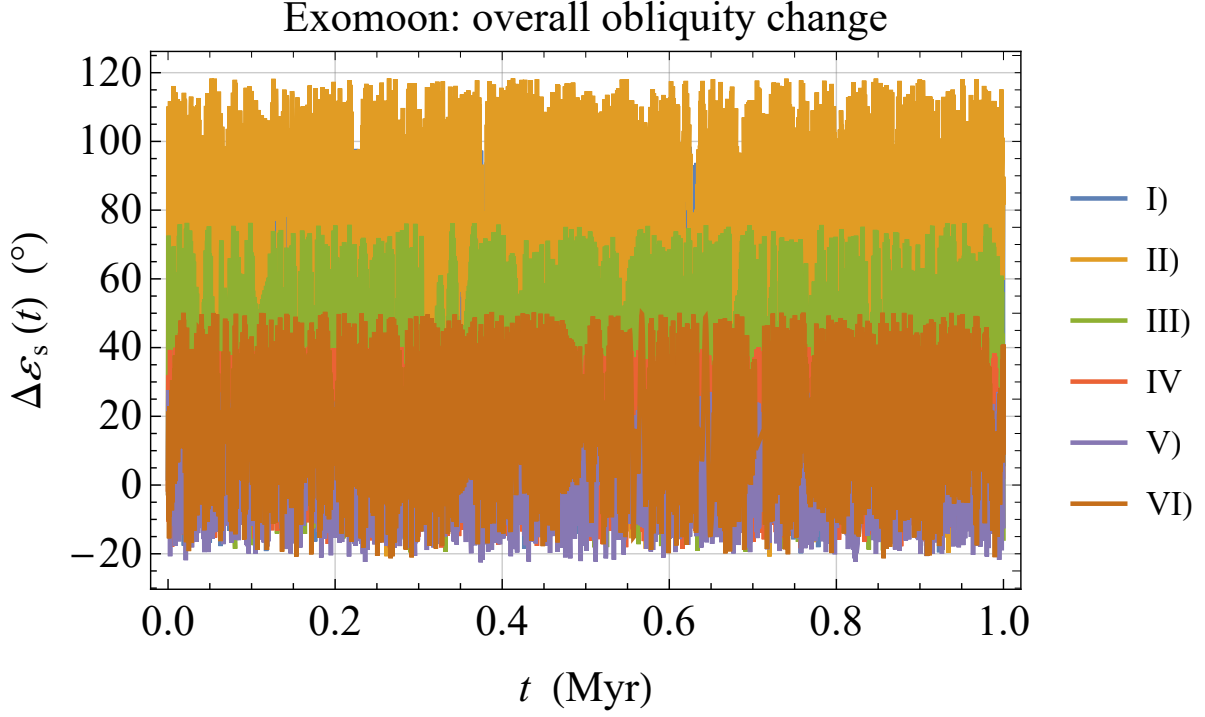


Fig. 9.— Numerically produced time series $\Delta\varepsilon_s(t) = \varepsilon_s(t) - \varepsilon_s^0$, in $^\circ$, of the general relativistic pN variation of the obliquity ε_s to the ecliptic plane of a putative exomoon orbiting a gaseous giant planet with the same physical properties of Jupiter. They were obtained by simultaneously integrating the orbit-averaged Equations (12)-(13), Equations (24)-(25), and Equations (46)-(47) for the rates of change of ε_s , α_s , Ω , I over 1 Myr. The initial conditions, corresponding to $\hat{\mathbf{L}}$, $\hat{\mathbf{S}}_p$, $\hat{\mathbf{S}}_s$ tilted almost identically to the ecliptic but located in different azimuthal planes, are listed in Table 3. For the exomoon, the mass, radius, normalized moment of inertia and mean density of the Earth were adopted, while $\omega_s = 1.1 n_b$ was assumed for its angular speed.

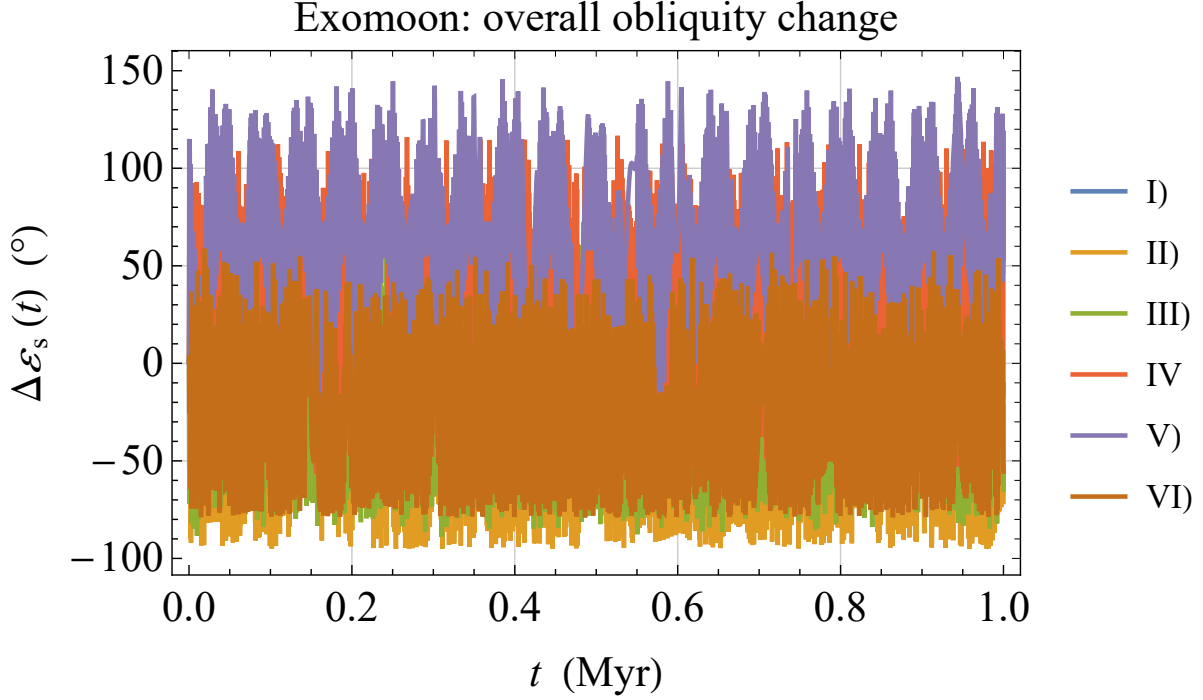


Fig. 10.— Numerically produced time series $\Delta \varepsilon_s(t) = \varepsilon_s(t) - \varepsilon_s^0$, in $^\circ$, of the general relativistic pN variation of the obliquity ε_s to the ecliptic plane of a putative exomoon orbiting a gaseous giant planet with the same physical properties of Jupiter. They were obtained by simultaneously integrating the orbit-averaged Equations (12)-(13), Equations (24)-(25), and Equations (46)-(47) for the rates of change of ε_s , α_s , Ω , I over 1 Myr. The initial conditions, corresponding to $\hat{\mathbf{L}}$, $\hat{\mathbf{S}}_p$, $\hat{\mathbf{S}}_s$ arbitrarily oriented, are listed in Table 4. For the exomoon, the mass, radius, normalized moment of inertia and mean density of the Earth were adopted, while $\omega_s = 1.1 n_b$ was assumed for its angular speed.

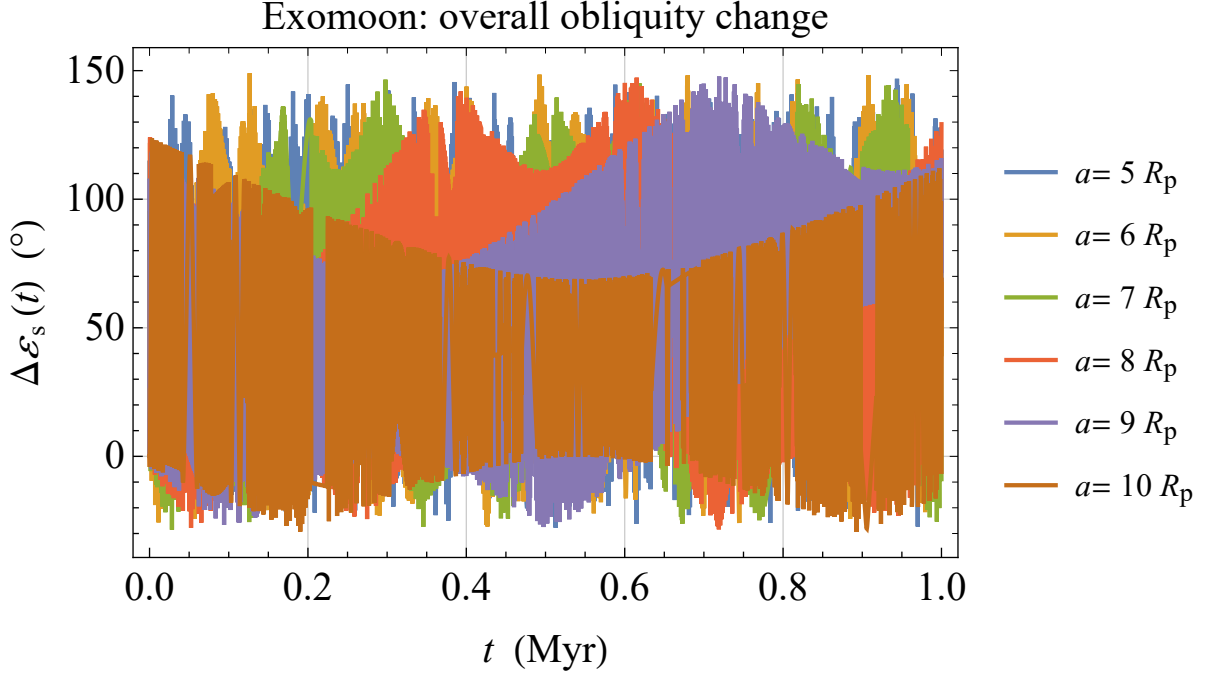


Fig. 11.— Numerically produced time series $\Delta \varepsilon_s(t) = \varepsilon_s(t) - \varepsilon_s^0$, in $^\circ$, of the general relativistic pN variation of the obliquity ε_s to the ecliptic plane of a putative exomoon orbiting a gaseous giant planet with the same physical properties of Jupiter. They were obtained by simultaneously integrating the orbit-averaged Equations (12)-(13), Equations (24)-(25), and Equations (46)-(47) for the rates of change of ε_s , α_s , Ω , I over 50 Myr. The initial spin-orbit configuration, common to all the runs, is listed in Table 5. For the exomoon, the mass, radius, normalized moment of inertia and mean density of the Earth were adopted, while $\omega_s = 1.1 n_b$ was assumed for its angular speed.

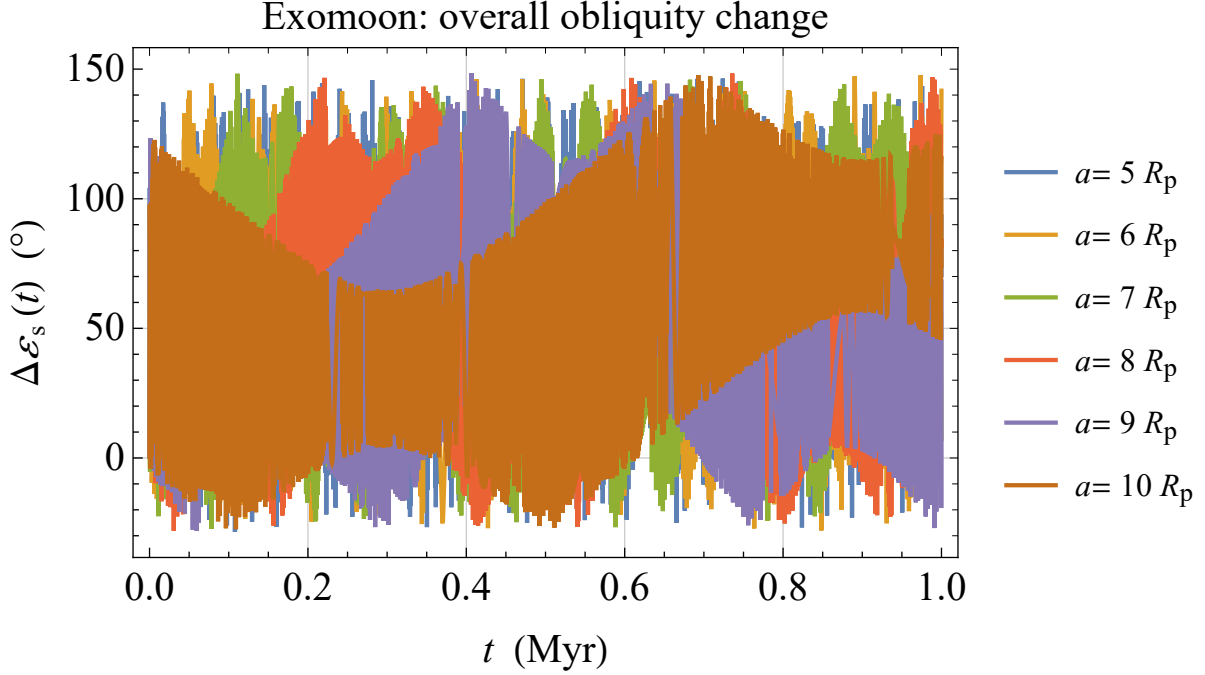


Fig. 12.— Numerically produced time series $\Delta\varepsilon_s(t) = \varepsilon_s(t) - \varepsilon_s^0$, in $^\circ$, of the general relativistic pN variation of the obliquity ε_s to the ecliptic plane of a putative exomoon orbiting a gaseous giant planet with the same physical properties listed in Table 6. They were obtained by simultaneously integrating the orbit-averaged Equations (12)-(13), Equations (24)-(25), and Equations (46)-(47) for the rates of change of ε_s , α_s , Ω , I over 50 Myr. The initial spin-orbit configuration, common to all the runs, is listed in Table 5. For the exomoon, the mass, radius, normalized moment of inertia and mean density of the Earth were adopted, while $\omega_s = 1.1 n_b$ was assumed for its angular speed.

6. The impact of the distant star and the obliquity to the planetocentric orbital plane

Until now, I kept the ecliptic plane fixed. Actually, the distant star S, assumed here pointlike and with the same mass of our Sun, does affect the orbital angular momentum \mathbf{W} of the revolution of the planet-satellite system \mathcal{S} about it by means of three torques proportional to its mass M_S two of which depend on J_2^s , J_2^p (Correia et al. 2011). Here, I investigate its possible influence on $\varepsilon_s = \arccos(\hat{\mathbf{S}}_s \cdot \hat{\mathbf{W}})$ by simultaneously integrating Eqs. (7)-(10) by (Correia et al. 2011) with the addition of the pN rates over the same time span of the figures in the previous Sections. I found that the inclusion of the torques by M_S does not substantially impact $\Delta\varepsilon_s$.

As far as the obliquity $\vartheta_s \doteq \arccos(\hat{\mathbf{S}}_s \cdot \hat{\mathbf{L}})$ of the satellite’s spin to the planetocentric orbital plane, which may play a role in the exomoon’s habitability because of the energy output from the planet itself (Heller & Barnes 2013), its variations $\Delta\vartheta_s$ are of no concern since their numerically integrated time series turn out to have negligible amplitudes.

7. Summary and Conclusions

I analytically and numerically studied the pN de Sitter and Lense-Thirring precessions of the spin of a spherically symmetric gyroscope freely moving in the deformed stationary spacetime of a massive rotating body for an arbitrary spin-orbit configuration. I applied my results to a putative exomoon orbiting different Jupiter-like gaseous giant planets, assumed to be at 1 au from a Sun-type main sequence star. In particular, I looked at the long-term pN variations $\Delta\varepsilon_s$ of the satellite's obliquity ε_s to the ecliptic plane, assumed fixed, with respect to its initial value ε_s^0 . Indeed, the axial tilt is a key parameter in constraining the capability of hosting and sustaining life over long time spans since it controls the insolation received directly from the star at a given body's latitude. Thus, fast and large temporal changes of ε_s , like those I found, may likely impact exomoons' habitability. Its detailed investigation from a climatological and planetological perspective is, however, outside the scopes of the present study.

First, I analytically derived orbit-averaged equations for the pN rates of change of the satellite's spin obliquity ε_s and azimuthal angle α_s along with the equations for the precessions of the orbital inclination I and longitude of ascending node Ω driven by both the classical quadrupole J_2^p and the pN Lense-Thirring spin component of the planetary gravitational field; the latter ones enter only indirectly $d\varepsilon_s/dt$ and $d\alpha_s/dt$. By initially neglecting the satellite's oblateness J_2^s which induces its own direct spin precession, its spin obliquity rate is, thus, purely pN.

Subsequently, the equations for ε_s , α_s , I , Ω were numerically integrated over 1 Myr. I started by varying the spin-orbit configuration by keeping the planetocentric distance from a Jupiter-like planet fixed to $5 R_p$. I considered four different scenarios. First, I assumed \hat{L} , \hat{S}_p , \hat{S}_s almost aligned with each other up to a few degrees: the ideal condition of perfect alignment of the three angular momenta would imply the absence of any spin precessions. I found the resulting ranges of variation $\varepsilon_s^{\max} - \varepsilon_s^{\min}$ large enough to be likely significant for habitability, amounting to $\approx 3^\circ - 17^\circ$. Then, I considered the cases in which \hat{L} , \hat{S}_p , \hat{S}_s a) Share almost the same azimuthal plane but are differently tilted to the ecliptic b) Are located in different azimuthal planes with almost the same axial tilts c) Are arbitrarily oriented in space. In all such cases, $\Delta\varepsilon_s$ experiences relevant variations up to tens and, sometimes, even hundreds degrees. All such integrations, covering 1 Myr, exhibit non-harmonic temporal patterns and a characteristic timescale of about 0.7 Myr. Finally, I made numerical integrations by varying also the exmoon's planetocentric distance from $5 R_p$ to $10 R_p$ for a given spin-orbit configuration. I found that all the curves for $\Delta\varepsilon_s$ retain essentially the same amplitudes, showing increasing characteristic timescales with distance.

I successfully tested my results with another set of runs over the same time spans based on the vectorial form of the spin and orbital precessions retrieved in the literature. The resulting times series agree with the previous ones up to less than a degree over the time span adopted.

I looked also at another parent planet for which the physical parameters of the existing exoplanet HD109906b were used. In particular, its mass is 11 times larger than that of Jupiter, and its oblateness J_2^p and spin angular momentum S_p can be up to 2.5 and 45 times larger than

the Jovian ones. The temporal patterns and the magnitudes of the resulting time series, calculated with the same sets of initial conditions, are similar to those for a Jupiter-like body, but their characteristic timescale is about the order of magnitude shorter. Indeed, the de Sitter frequency of a HD109906b-type planet is just about 10 times larger than that of Jupiter for the same planetocentric distances.

Then, I studied the impact of the own oblateness J_2^s of the exomoon on ε_s by adding its Newtonian torque to the numerically integrated equations for the spin rates after having analytically worked out its spin rates as well. In calculating the satellite's quadrupole mass moment and spin angular momentum S_s , I assumed the relevant physical parameters of the Earth by allowing for the exomoon's angular rotational speed ω_s a value, say, 10% larger than that of the planetocentric mean motion n_b . As a result, I obtained very high frequency signatures of comparable amplitudes to the pN ones to which they are superimposed without canceling them. Also in this case, the numerical integrations of the analytically worked out averaged spin rate equations agree with those performed with their vectorial form.

I tested the assumption that the plane of the astrocentric motion of the planet-satellite binary can be considered fixed by adding the torques arising from the action of the distant star to the dynamical model to be integrated. The resulting time series for $\Delta\varepsilon_s$ do not noticeably differ from those previously obtained by keeping the ecliptic fixed.

Finally, I investigated also the classical and pN variations of the obliquity of the exomoon's spin with respect to the plane of its orbit around the host planet, which may be another relevant factor in the total energy balance because of the irradiation from the planet itself due to both the reflected sunlight and the infrared radiation. It turned out to be negligible.

As directions for future work, a further effect which is likely worth of further investigations is the impact of the tidal torques which, among other things, tend to align the orbital angular momentum of the planetocentric orbit with the planet and satellite's spins in order to see if, and to which extent, they are effectively counterbalanced by the relativistic signatures obtained here, especially when their characteristic frequencies increase because of a heavier primary than Jupiter.

In conclusion, the pN temporal variations of the tilt of the exomoon's spin axis to the plane of the planet-satellite's orbit around a distant Sun-like main sequence star are fast and large enough to have most likely a significant impact on its habitability for a variety of different spin-orbit configurations, even when the high frequency modulation due to the satellite's own oblateness is taken into account. It is true also in the scenario in which the satellite's spin is almost aligned with the planetary one and with the planetocentric orbital angular momentum up to offsets of a few degrees. Future climatological and planetological studies on the habitability of exomoons should include also such effects in the overall budget of the dynamical constraints to life sustainability.

Data availability

No new data were generated or analysed in support of this research.

REFERENCES

- Armstrong J. C., Barnes R., Domagal-Goldman S., Breiner J., Quinn T. R., Meadows V. S., 2014, *AsBio*, 14, 277
- Armstrong J. C., Leovy C. B., Quinn T., 2004, *Icar*, 171, 255
- Asada H., Futamase T., 1997, *PThPS*, 128, 123
- Barker B. M., O’Connell R. F., 1975, *PhRvD*, 12, 329
- Barnes J. W., O’Brien D. P., 2002, *ApJ*, 575, 1087
- Barr A. C., 2016, *AstRv*, 12, 24
- Barr A. C., Bruck Syal M., 2017, *MNRAS*, 466, 4868
- Blanchet L., 2003, in *Proceedings of the Twelfth Workshop on General relativity and Gravitation in Japan*, Shibata M., Eriguchi Y., Taniguchi K., Nakamura T., Tomita K., eds., The University of Tokyo, Komaba, Tokyo, pp. 8–23
- Bourda G., Capitaine N., 2004, *A&A*, 428, 691
- Breton R. P. et al., 2008, *Sci*, 321, 104
- Brumberg V. A., 1991, *Essential Relativistic Celestial Mechanics*. Adam Hilger, Bristol
- Bryan M. L., Ginzburg S., Chiang E., Morley C., Bowler B. P., Xuan J. W., Knutson H. A., 2020, *ApJ*, 905, 37
- Cabrera J., Schneider J., 2007, *A&A*, 464, 1133
- Campante T. L. et al., 2016, *ApJ*, 819, 85
- Correia A. C. M., Laskar J., Farago F., Boué G., 2011, *CeMDA*, 111, 105
- Correia A. C. M., Rodríguez A., 2013, *ApJ*, 767, 128
- Damour T., Schafer G., 1988, *NCimB*, 101, 127
- Damour T., Taylor J. H., 1992, *PhRvD*, 45, 1840
- de Pater I., Lissauer J. J., 2015, *Planetary Sciences*. Cambridge University Press, New York
- de Sitter W., 1916, *MNRAS*, 77, 155
- Debono I., Smoot G. F., 2016, *Univ*, 2, 23
- Deeg H. J., Belmonte J. A., 2018, *Handbook of Exoplanets*. Springer, Cham

- Dickey J. O. et al., 1994, *Sci*, 265, 482
- Dobos V., Heller R., Turner E. L., 2017, *A&A*, 601, A91
- Domingos R. C., Winter O. C., Yokoyama T., 2006, *MNRAS*, 373, 1227
- Efroimsky M., Makarov V. V., 2013, *ApJ*, 764, 26
- Everitt C. W. F. et al., 2011, *PhRvL*, 106, 221101
- Everitt C. W. F. et al., 2015, *CQGra*, 32, 224001
- Fokker A. D., 1920, *KNAB*, 29, 611
- Forgan D., Kipping D., 2013, *MNRAS*, 432, 2994
- Forgan, D., 2019, *IJA*, 18, 510
- Fox C., Wiegert P., 2021, *MNRAS*, 501, 2378
- Helled R., Anderson J. D., Schubert G., Stevenson D. J., 2011, *Icar*, 216, 440
- Heller R., Barnes R., 2013, *AsBio*, 13, 18
- Heller R., Leconte J., Barnes R., 2011, *A&A*, 528, A27
- Heller R. et al., 2014, *AsBio*, 14, 798
- Heller, R., 2012, *A&A*, 545, L8
- Hill M. L., Kane S. R., Seperuelo Duarte E., Kopparapu R. K., Gelino D. M., Wittenmyer R. A., 2018, *ApJ*, 860, 67
- Hinkel N. R., Kane S. R., 2013, *ApJ*, 774, 27
- Hofmann F., Müller J., 2018, *CQGra*, 35, 035015
- Iess L. et al., 2018, *Natur*, 555, 220
- Iorio L., 2017, *EPJC*, 77, 439
- Irwin L. N., Schulze-Makuch D., 2020, *Univ*, 6, 130
- Kaltenegger L., 2010, *ApJ*, 712, L125
- Kaltenegger L., 2017, *ARA&A*, 55, 433
- Kerr R. A., 1987, *Sci*, 235, 973
- Kilic C., Raible C. C., Stocker T. F., 2017, *ApJ*, 844, 147

- Kipping D. M., 2009a, MNRAS, 392, 181
- Kipping D. M., 2009b, MNRAS, 396, 1797
- Kipping D. M., Bakos G. Á., Buchhave L., Nesvorný D., Schmitt A., 2012, ApJ, 750, 115
- Kipping D. M., Forgan D., Hartman J., Nesvorný D., Bakos G. Á., Schmitt A., Buchhave L., 2013a, ApJ, 777, 134
- Kipping D. M., Fossey S. J., Campanella G., 2009, MNRAS, 400, 398
- Kipping D. M., Hartman J., Buchhave L. A., Schmitt A. R., Bakos G. Á., Nesvorný D., 2013b, ApJ, 770, 101
- Kopal Z., 1959, Close binary systems. Chapman & Hall, London
- Kramer M., 2012, in The Twelfth Marcel Grossmann Meeting. Proceedings of the MG12 Meeting on General Relativity, Damour T., Jantzen R., Ruffini R., eds., World Scientific, Singapore, pp. 241–260
- Laskar J., Joutel F., Robutel P., 1993, Natur, 361, 615
- Laskar J., Robutel P., Joutel F., et al., 2004, A&A, 428, 261
- Leconte J., Lai D., Chabrier G., 2011, A&A, 528, A41
- Lingam M., Loeb A., 2020, IJA, 19, 210
- Linsenmeier M., Pascale S., Lucarini V., 2015, P&SS, 105, 43
- Lissauer J. J., 2012, NewAR, 56, 1
- Lissauer J. J., Barnes J. W., Chambers J. E., 2012, Icar, 217, 77
- Malamud U., Perets H. B., Schäfer C., Burger C., 2020, MNRAS, 492, 5089
- Martínez-Rodríguez H., Caballero J. A., Cifuentes C., Piro A. L., Barnes R., 2019, ApJ, 887, 261
- Mashhoon B., 2001, in Reference Frames and Gravitomagnetism, Pascual-Sánchez J. F., Floría L., San Miguel A., Vicente F., eds., World Scientific, Singapore, pp. 121–132
- Mignard F., 1979, M&P, 20, 301
- Milankovitch M., 1941, Kanon der Erdbestahlung und seine Anwendung auf das Eiszeitenproblem. Belgrad Königliche Serbische Akademie
- Misner C. W., Thorne K. S., Wheeler J. A., 2017, Gravitation. Princeton University Press, Princeton

- Mitrovica J. X., Forte A. M., 1995, *GeoJI*, 121, 21
- Murray C. D., Dermott S. F., 2000, *Solar System Dynamics*. Cambridge: Cambridge Univ. Press
- Ohanian H., Ruffini R., 2013, *Gravitation and Spacetime*. Third Edition. Cambridge University Press, Cambridge
- Pais M. A., Le Mouél J. L., Lambeck K., Poirier J. P., 1999, *E&PSL*, 174, 155
- Perryman M., 2018, *The Exoplanet Handbook*. Second edition. Cambridge Univ. Press, Cambridge
- Petit G., Luzum B., et al., 2010, *IERS Technical Note*, 36, 1
- Poisson E., Will C. M., 2014, *Gravity*. Cambridge: Cambridge Univ. Press
- Porter S. B., Grundy W. M., 2011, *ApJ*, 736, L14
- Pugh G., 1959, Proposal for a Satellite Test of the Coriolis Prediction of General Relativity. Research Memorandum 11, Weapons Systems Evaluation Group, The Pentagon, Washington D.C.
- Quarles B., Barnes J. W., Lissauer J. J., Chambers J., 2019, *AsBio*, 20, 73
- Quarles B., Li G., Lissauer J. J., 2019, *ApJ*, 886, 56
- Ragozzine D., Wolf A. S., 2009, *ApJ*, 698, 1778
- Rindler W., 2001, *Relativity: special, general, and cosmological*. Oxford University Press, Oxford, UK
- Rodenbeck K., Heller R., Gizon L., 2020, *A&A*, 638, A43
- Sartoretti P., Schneider J., 1999, *A&AS*, 134, 553
- Sasaki T., Stewart G. R., Ida S., 2010, *ApJ*, 714, 1052
- Schiff L., 1960, *PhRvL*, 4, 215
- Schneider J., Lainey V., Cabrera J., 2015, *IJAsB*, 14, 191
- Schouten W. J. A., 1918, *KNAB*, 27, 214
- Schulze-Makuch D., Bains W., 2018, *NatAs*, 2, 432
- Schwieterman E. W. et al., 2018, *AsBio*, 18, 663
- Seager S., 2011, *Exoplanets*. University of Arizona Press, Tucson

- Shan Y., Li G., 2018, *AJ*, 155, 237
- Soffel M. et al., 2003, *AJ*, 126, 2687
- Soffel M. H., Han W.-B., 2019, *Applied General Relativity, Astronomy and Astrophysics Library*.
Springer Nature Switzerland, Cham
- Sterne T. E., 1939, *MNRAS*, 99, 451
- Teachey A., Kipping D. M., 2018, *SciA*, 4, eaav1784
- Teachey A., Kipping D. M., Schmitt A. R., 2018, *AJ*, 155, 36
- Thorne K. S., MacDonald D. A., Price R. H., eds., 1986, *Black Holes: The Membrane Paradigm*.
Yale University Press, Yale
- Tjoa J. N. K. Y., Mueller M., van der Tak F. F. S., 2020, *A&A*, 636, A50
- Trifonov T. et al., 2020, *A&A*, 638, A16
- Will C. M., 2008, *ApJL*, 674, L25
- Will C. M., 2018, *Theory and Experiment in Gravitational Physics. Second edition*. Cambridge
University Press, Cambridge
- Williams D. M., Kasting J. F., 1997, *Icar*, 129, 254
- Williams D. M., Kasting J. F., Wade R. A., 1997, *Natur*, 385, 234
- Williams J. G., Folkner W. M., 2009, in *IAU Symposium #261*, American Astronomical Society,
Vol. 261, p. 882
- Williams J. G., Newhall X. X., Dickey J. O., 1996, *PhRvD*, 53, 6730
- Zollinger R. R., Armstrong J. C., Heller R., 2017, *MNRAS*, 472, 8